



**FEASIBILITY OF USING CLASSIFICATION ANALYSES TO DETERMINE  
TROPICAL CYCLONE RAPID INTENSIFICATION**

THESIS

Jonathan W. Leffler, Captain, USAF

AFIT/GM/ENP/04-07

**DEPARTMENT OF THE AIR FORCE  
AIR UNIVERSITY**

**AIR FORCE INSTITUTE OF TECHNOLOGY**

---

---

**Wright-Patterson Air Force Base, Ohio**

APPROVED FOR PUBLIC RELEASE; DISTRIBUTION UNLIMITED.

The views expressed in this thesis are those of the author and do not reflect the official policy or position of the United States Air Force, Department of Defense, or the United States Government.

AFIT/GM/ENP/04-07

FEASIBILITY OF USING CLASSIFICATION ANALYSES TO DETERMINE  
TROPICAL CYCLONE RAPID INTENSIFICATION

THESIS

Presented to the Faculty

Department of Engineering Physics

Graduate School of Engineering and Management

Air Force Institute of Technology

Air University

Air Education and Training Command

In Partial Fulfillment of the Requirements for the

Degree of Master of Science in Meteorology

Jonathan W. Leffler, BS

Captain, USAF




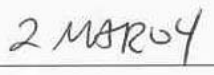
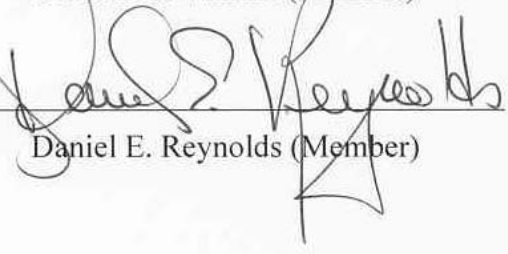
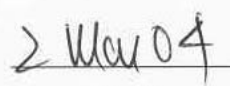
March 2004

APPROVED FOR PUBLIC RELEASE; DISTRIBUTION UNLIMITED.

FEASIBILITY OF USING CLASSIFICATION ANALYSES TO DETERMINE  
TROPICAL CYCLONE RAPID INTENSIFICATION

Jonathan W. Leffler, BS  
Captain, USAF

Approved:

 _____ Ronald P. Lowther (Chairperson)	 _____ Date
 _____ Michael K. Walters (Member)	 _____ Date
 _____ Daniel E. Reynolds (Member)	 _____ Date

## **Abstract**

Tropical cyclone intensity techniques developed by Dvorak have thus far been regarded by tropical meteorologists as the best identification and forecast schemes available using satellite imagery. However, in recent years, several ideologies have arisen which discuss alternative means of determining typhoon rapid intensification or weakening in the Pacific. These theories include examining channel outflow patterns, potential vorticity superposition and anomalies, tropical upper tropospheric trough interactions, environmental influences, and upper tropospheric flow transitions.

It is now possible to data mine these atmospheric parameters thought partly responsible for typhoon rapid intensification and weakening to validate their usefulness in the forecast process. Using the latest data mining software tools, this study used components of NOGAPS analyses along with selected atmospheric and climatological predictors in classification analyses to create conditional forecast decision trees. The results of the classification model show an approximate  $R^2$  of 0.68 with percent error misclassifications of 13.5% for rapidly weakening typhoon events and 21.8% for rapidly intensifying typhoon events. In addition, a merged set of suggested forecast splitting rules was developed. By using the three most accurate predictors from both intensifying and weakening storms, the results validate the notion that multiple parameters are responsible for rapid changes in typhoon development.

## **Acknowledgements**

There are many people whom I would like to thank on this project. First and foremost, I thank the Lord for giving me wisdom to complete the research, humility to keep trying, and patience to work with outcomes, which had not been foreseen. I would also like to thank my advisor, Lt Col Ron Lowther, and my other committee members, Lt Col Michael Walters and Professor Dan Reynolds, for their insight and willingness to help me when I was unable to see the road ahead. I am also truly indebted to my wonderful wife and brand new daughter for the hundreds of hours I've spent locked up in an office or away from home. Thank you for your understanding and loyalty.

This thesis work would not have been accomplished without the help of Capt Steve Vilpors of the Joint Typhoon Warning Center and Jeff Zautner of the Air Force Combat Climatology Center. Thank you both for answering all my questions and providing the data for this study. In addition, I would like to thank Mikhail Golovnya of Salford Systems, Inc., who persisted in helping me master concepts of the CART data mining software. Finally, to my classmates who have supported me from the beginning, thank you for your teamwork and your knowledge during these past 18 months. It has definitely been an experience I will always remember.

Jonathan W. Leffler

## Table of Contents

Abstract .....	iv
Acknowledgements .....	v
List of Figures .....	viii
List of Tables .....	x
I. Introduction .....	1
1.1 Statement of the Problem .....	2
1.2 Research Objectives .....	3
1.3 Research Approach .....	7
II. Literature Review .....	9
2.1 Dvorak Technique .....	9
2.2 Channel Outflow Patterns and Opposite Hemisphere Effects .....	14
2.3 Potential Vorticity Superposition and Anomalies .....	17
2.4 Tropical Upper Tropospheric Trough Interactions .....	19
2.5 Environmental Influences .....	23
2.5.1 Sea Surface Temperatures .....	23
2.5.2 Effects of Vertical Shear .....	24
2.5.3 Air Sea Interactions .....	27
2.6 Upper Tropospheric Flow Transitions .....	28
III. Methodology .....	30
3.1 Introduction .....	30
3.2 Data Acquisition .....	30
3.2.1 Storm Selection .....	30
3.2.2 Best Track Data .....	31
3.2.3 NOGAPS Model .....	32
3.2.4 Sea Surface Temperatures .....	34
3.2.5 CPC Teleconnection Indices .....	35
3.3 CART Overview .....	36
3.3.1 Methods .....	38
3.3.1.1 Tree Splitting Methods .....	38
3.3.1.2 Pruning .....	41
3.3.1.3 Cross Validation .....	42
3.3.1.4 Improvement Scores .....	43

3.3.1.5 Class Assignments .....	44
3.3.2 Research Predictors .....	45
3.4 Statistical Overview .....	49
3.4.1 Introduction .....	49
3.4.2 Simple Linear Regression .....	50
IV. Analysis and Results .....	53
4.1 Introduction .....	53
4.2 Regression Analysis of NOGAPS and Best Track Data .....	53
4.3 Classification Tree Analysis .....	55
4.3.1 Best Method Determination .....	55
4.3.2 Alternate Target Classification Tree Results .....	62
4.3.3 Primary Target Classification Tree Results .....	65
4.4 Supplement to the Intensity Analysis Worksheet and Verification .....	78
V. Conclusions and Recommendations .....	83
5.1 Conclusions .....	83
5.2 Recommendations .....	86
5.2.1 Recommendations to JTWC .....	86
5.2.2 Future Research Recommendations .....	88
Appendix A: MATLAB Linear Interpolation of Grid Points Program .....	90
Appendix B: MATLAB Calculation of Wind Shear Program .....	92
Appendix C: Complete Set of Splitting Rules .....	98
Acronyms .....	102
Bibliography .....	104
Vita .....	108



## List of Figures

Figure	Page
1. Intensity change curves of the model .....	10
2. Common TC patterns and corresponding T-numbers .....	11
3. Examples of TC Patterns .....	11
4. Example of a LOG10 spiral graph .....	12
5. Corresponding LOG10 spiral graph reference .....	12
6. Variety of outflow patterns associated with TC intensification for Northern Hemisphere cases.....	15
7. Six types of interactions between a TC and its surroundings .....	21
8. 1997 Northwest Pacific TC tracks .....	25
9. 1999 Northwest Pacific TC tracks .....	26
10. 2001 Northwest Pacific TC tracks .....	26
11. Sample Gini splitting function .....	39
12. Sample Twoing splitting function .....	39
13. Graphical depiction of 10-fold cross validation .....	43
14. Example of an improvement score .....	44
15. Classification tree for CAT STSS .....	63
16. Classification tree for CAT STDS .....	63
17. Classification tree for TGT (Class 2).....	66
18. Classification tree for TGT (Class 1).....	66
19. Classification tree for TGT (Class 0).....	67
20. New classification tree for TGT (Class 2) .....	70

21. New classification tree for TGT (Class 1) .....	70
22. New classification tree for TGT (Class 0) .....	71
23. Splitters for new classification tree.....	71
24. JMP distribution of Class 1.....	75
25. JMP distribution of Class 2.....	75

## List of Tables

Table	Page
1. Empirical relationship between CI number and MWS, and the relationship between the T-number and MSLP .....	14
2. Selected typhoons from 1997, 1999, and 2001 .....	31
3. Sample best track data for TC 04 .....	32
4. NOGAPS model fields .....	33
5. Storms with missing model fields .....	34
6. List of CART predictors .....	46
7. Rules for categorical predictors .....	47
8. Categorical values for predictor rules .....	47
9. Initial regression analysis of NOGAPS and BT .....	55
10. Initial screening of relative cost .....	56
11. Initial screening of percent error misclassification .....	56
12. Initial screening of percent prediction success .....	57
13. Total counts of initial screening .....	59
14. Average percent error misclassification .....	59
15. Percent error misclassification for CAT STSS .....	61
16. Percent error misclassification for CAT STDS .....	61
17. Percent error misclassification for CH OUT .....	62
18. Terminal node details for CAT STSS .....	63
19. Terminal node details for CAT STDS .....	63
20. Splitting rules for CAT STSS .....	64

21. Splitting rules for CAT STDS .....	64
22. Terminal node details for TGT .....	67
23. Variable importance for TGT .....	69
24. Refined variable importance for TGT .....	69
25. New terminal node details for TGT .....	73
26. Class 1 and Class 2 splitting rules .....	74
27. JMP moments table for class distributions .....	74
28. Criteria used to determine validity of splitting rules .....	77
29. TC intensity analysis worksheet .....	80
30. Suggested forecast splitting rules .....	80
31. Verification counts of the forecast splitting rules .....	81
32. Accuracy of the forecast splitting rules .....	81

# FEASIBILITY OF USING CLASSIFICATION ANALYSES TO DETERMINE TROPICAL CYCLONE RAPID INTENSIFICATION

## I. Introduction

For the past 45 years, the Joint Typhoon Warning Center (JTWC), currently located in Hawaii, has been responsible for the observation, analysis, forecast, and public dissemination of tropical cyclone warnings in the western and southern Pacific and Indian Ocean basins. During this time, numerous tropical cyclones have impacted Department of Defense assets, stretching from Hawaii to Japan. A tropical cyclone (TC), commonly known in the western Pacific Ocean as a typhoon, can vary in strength and is categorized according to its maximum wind speeds. A tropical depression (TD) is defined by winds  $\leq 17 \text{ m s}^{-1}$ , a tropical storm (TS) is defined by winds 18 to  $32 \text{ m s}^{-1}$ , and a typhoon is defined by winds  $\geq 33 \text{ m s}^{-1}$ . There is also a special category of TC called super typhoon, which requires winds  $\geq 65 \text{ m s}^{-1}$ . This is comparable to a Category IV+ hurricane on the Saffir-Simpson hurricane scale (Glickman et al. 2000).

During the past decade, the precision of typhoon forecast tracks has improved greatly, thanks to the help of advances in numerical modeling, such as the Systematic Approach to Tropical Cyclone Forecasting Aid (SAFA) program, and computer systems such as the Automated Tropical Cyclone Forecasting (ATCF) system (Vilpors personal correspondence 2003). However, one of the main concerns of JTWC has been the ability to accurately predict intensity changes of tropical cyclones in advance.

“In the early days of meteorological satellite programs, the feasibility of using satellite imagery for tropical cyclone analysis was recognized” (Sadler 1964). In 1973, Vernon Dvorak developed a technique by which intensification could be predicted based on the current configuration of cloud features (Dvorak 1974). JTWC has been using this method as its main technique to analyze current and forecast intensity factors. However, during the past few years, several researchers have proposed other means of forecasting tropical cyclone intensification. Some of these proposals include using channel outflow patterns, potential vorticity superposition and anomalies, tropical upper tropospheric trough (TUTT) interaction, environmental influences, and upper tropospheric flow transitions. The following chapters explore these inner workings of tropical cyclone intensification.

### *1.1 Statement of the Problem*

The Joint Typhoon Warning Center has become relatively proficient in forecasting the movement of tropical cyclones. However, they lack substantial expertise in predicting tropical cyclone intensification. Specifically, they have requested tools for tropical cyclone intensity forecasting using synoptic patterns defined by water vapor imagery, observations, and model field analyses. JTWC also requested a guideline for slow, climatological and rapid deepeners to include the effects of tropical upper tropospheric trough cells on intensification trends. The current procedure for forecasting intensification has been the Dvorak Technique, from which the T-number is computed. The T-number is simply a numeric designator for the current intensity of a tropical

cyclone. For a slowly intensifying tropical cyclone, the T-number rises 0.5 per day; a steady or climatologically intensifying cyclone increases at 1.0 T-number per day; and a rapidly intensifying system rises 1.5 T-number or more per day.

Although this technique is considered quite accurate, it can be highly subjective depending on the lifecycle of the tropical cyclone and how well its central and banding features are defined. The overall premise of the technique relies on cloud pattern recognition and comparison with a model of anticipated intensity trends. The technique does not take TUTT cell interactions into account, therefore alternative methods must be devised.

## *1.2 Research Objectives*

The overall goal of this thesis is to data mine atmospheric parameters responsible for typhoon rapid intensification and weakening and to validate the usefulness of using these parameters in the forecast process. This thesis examines a variety of mechanisms thought responsible for tropical cyclone intensification. Chapter 2 discusses these parameters individually, exploring the inner workings of tropical cyclone intensification, and illustrating relationships between the different parameters. Chapter 3 portrays the methodology involved in this research, from selection of typhoons and predictors to a quick overview of simple linear regression. Chapter 4 is devoted to analysis and results while Chapter 5 yields conclusions to this thesis and recommendations for future work.

The first objective of this research is to gather all types of satellite imagery (visible, water vapor, and infrared) since satellite interrogation is one of the primary tools

in analyzing Northwest Pacific typhoons. This imagery is archived by the Naval Research Laboratory (NRL), according to each typhoon event, as well as by the Australian Bureau of Meteorology (BOM). In addition, the imagery should include the entire lifetime of the tropical cyclone, if possible, from tropical depression to typhoon strength. Still satellite imagery is used in the analysis, however animation loops are also beneficial in order to show changes over time. Although emphasis has been placed on water vapor imagery (given that this particular channel depicts the upper portions of the atmosphere), visible and infrared imagery are not excluded due to their unique perspective of the events. Visible imagery can show both upper and lower level cloud fields (inflows, outflows, and convective activity), whereas infrared imagery can isolate the typhoon core when the eye is obscured by cloud cover. Infrared imagery can also show areas of enhanced convection due to colder cloud tops. This knowledge proves very useful in determining whether a typhoon is gaining or losing strength.

The second objective of the research is to collect the best track data from JTWC. The best track data are reanalyses of every typhoon event during the year in each of the ocean basins. These data include six hourly fixes on each storm to include latitude, longitude, maximum sustained wind speed (kts), and minimum sea level pressure (mb). Best track data serve as the official record of the typhoon's progress, both in intensity changes and movement. This information is absolutely essential since it provides the closest ground truth for any analysis and a basis from which to build a forecasting methodology. Several graphical depictions are developed from the best track data in order to provide a quick look at key timeframes in typhoon lifecycles. Also, the different



mechanisms which cause increases or decreases in central surface pressure can be compared to determine any relationships which prove helpful during analysis.

A third objective is to collect the Navy Operational Global Atmospheric Prediction System (NOGAPS) model field analyses. NOGAPS is the preferred model in this analysis because its global domain includes the Pacific basin, and it is available from the Fleet Numerical Meteorology and Oceanography (FLENUMMETOC) Detachment at the Air Force Combat Climatology Center (AFCCC) for the 1997, 1999, and 2001 typhoon seasons. These years are selected due to climatological importance, discussed in the fourth objective. The National Centers for Environmental Prediction (NCEP) also archive model fields such as temperature, pressure, etc. which are available for reanalysis. These fields are a vital link to the research because the entire area of interest is open ocean, and there are no surface based observations from which to draw data. Also, the usage of routine upper air soundings is limited, therefore model fields become the dominant analysis tool. In addition, there are no longer aircraft reconnaissance flights such as those which currently exist over the Atlantic basin. Hence all of the available fields (temperature, pressure, moisture, winds, etc.) are necessary components in the data set, given the aforementioned constraints. Some of the proposed mechanisms for intensification rely on derived model fields (potential vorticity, etc.), and those parameters are obtained as well, if they are easily computed or archived.

The fourth objective of the research is to incorporate climatological and teleconnection indices into the data set for predictive analyses. Climatological conditions such as El Niño (EN) and La Niña (LN) periods are included to see what effects they contribute to tropical cyclone intensification. EN and LN events profoundly alter

tropospheric circulation in the western North Pacific. “Alteration of vertical shear causes tropical cyclones to form farther south and east than normal during EN events, and farther north and west than normal during LN events” (Ford 2000). Sea surface temperature patterns are also a major factor in determining TC development areas. “These formation site differences lead to longer tracks and stronger tropical cyclones during EN, and shorter tracks and weaker tropical cyclones during LN events” (Ford 2000). Recent EN years include 1994-95 and 1997-98, while recent LN years include 1996-97 and 1998-99. In order to manage the amount of typhoon data and compare with the availability of NOGAPS and National Climatic Data Center (NCDC) model fields, 1997 is selected as the EN year and 1999 as the LN year for this analysis. In contrast, 2001 is selected as a neutral (NU) year, where neither EN nor LN regimes dominated.

The fifth objective of the research is to examine relationships between the proposed intensification mechanisms, which is done via classification and regression tree (CART) analyses. CART is the backbone of the research because the main goal rests on using a variety of predictors to determine typhoon intensity trends. Other researchers have already shown that several mechanisms result in the intensification or dissipation of the storms (Chen and Gray 1985, Davidson and Kar 2002, DeMaria 1996, Evans 1993, Hanley et al. 2001, Holland 1997, Merrill 1987, Molinari et al. 1998, Sadler 1975, Sadler 1978, Sikora et al. 1976). If a pattern of intensification exists among different atmospheric parameters, then understanding this pattern will help JTWC improve its intensity forecasts. Using CART software will help isolate patterns in the data. Since no one parameter is the ultimate factor in strengthening or weakening a typhoon, a synergy

between several predictors may be responsible for these rapid changes during the lifecycle.

### *1.3 Research Approach*

The approach to this research is two fold. First, an objective analysis is accomplished by gathering archived numerical data such as pressure, wind, sea surface temperature, wind shear, etc. All of these fields are computed by models or observed by satellite remote sensing. Second, a subjective analysis is performed to fill in the gaps where objective analyses are not possible. For example, in examining channel outflow patterns or TUTT interactions, this determination is a subjective call by the analyst. The NOGAPS model does not generate a field for outflows nor upper tropospheric interactions. CART data mining brings these various ideologies of intensification together.

CART analyses are designed to find patterns in sets of data. Based upon predetermined conditions, these analyses can map the anticipated trend of an event (i.e., they build conditional forecast decision trees). They use various functions and splitting rules to determine how a tree is developed into subcategories, called nodes. Once a terminal node is reached, meaning that the data can no longer be split further, conclusions can be drawn from information contained in different nodes, and a pattern in the data could be recognized. The splitting process occurs from a set of predictors, defined at the beginning of the tree, which result in terminal nodes containing a certain percentage of the data. This particular process is outlined in Chapter 3.

One main challenge of the research is to develop a variety of predictors to be analyzed by CART. Some of these predictors such as potential vorticity anomalies, sea surface temperatures, and vertical shear are already employed in current numerical modeling schemes. Other predictors such as channel outflow patterns, TUTT interactions, and upper tropospheric flow transitions are apparent in satellite imagery; however, they are not analyzed as specific model fields. Their contributions are mostly of a synoptic nature and not derived from numerical methods. The key is to determine how to bridge together a model analysis field with a synoptic depiction while using the data mining software.

The second main challenge is to study how CART analyzes these relationships and to compare the outcomes with the trends in the best track data. Each combination of predictors results in a decision tree. Once the data are analyzed by CART, the different decision trees are compared, and a recommendation is made based upon which predictors are found to have the greatest influence on the target (rapid intensification or rapid weakening). In order to improve the overall forecast process, it is important to enhance the current consensus forecasting methods by JTWC with the recursive splitting methods done by CART. Although the data mining will most likely produce non-traditional results, the interpretation of these results will be one of the elements required to enhance intensity forecasting techniques.

## II. Literature Review

### *2.1 Dvorak Technique*

The technique developed by Dvorak has thus far been regarded, by tropical meteorologists, as the best intensity identification scheme using satellite imagery. Its overall basis is to compare the tropical cyclone's current central features (CF) and banding features (BF) with a model of tropical cyclone development. "The CF are those which appear within the broad curve of the comma band and either surround or cover the cloud system center. The BF refer to only that part of the comma cloud band that is overcast and curves evenly around the CF" (Dvorak 1974). The model depicts a variety of tropical cyclone intensity changes and describes how the BF and CF change over time (Dvorak 1974). Given the current characteristics of the CF and BF, a forecaster can compare the satellite imagery to a matrix of possible curves. These curves are related to the T-number, which is simply a numeric designator for the current intensity of the tropical cyclone. For a slowly intensifying tropical cyclone, one would expect the T-number to rise 0.5 per day; a steady or climatologically intensifying cyclone would increase 1.0 T-number per day; and a rapidly intensifying system would grow 1.5 T-number or more per day. Figure 1 shows trends of T-numbers and the associated rates of intensification.

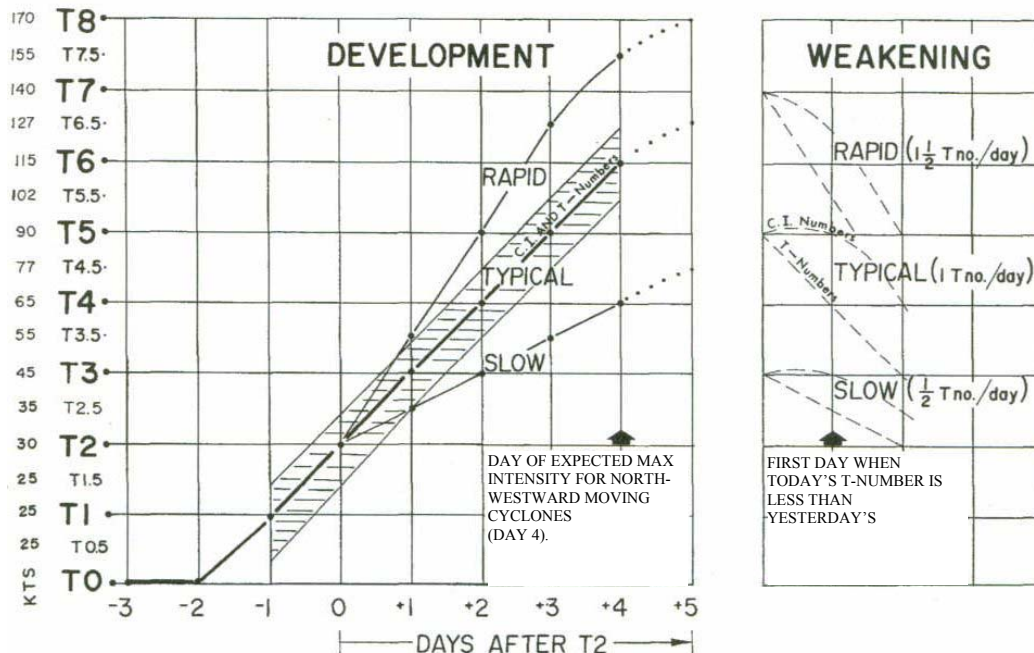


Figure 1. Intensity change curves of the model. The hatched area surrounding the typical curve is used to represent “intensity” as a zone one T-number wide (modified from Dvorak 1974 and used with permission of the American Meteorological Society (AMS)).

Another important typhoon characteristic the forecaster should recognize is the central dense overcast (CDO). The CDO is defined as the region of dense cloud near the core of a tropical cyclone (Glickman et al. 2000). The CDO plays an important role because it helps determine the intensity trend of the tropical cyclone. If the CDO is initially small, then becomes larger and more circular over time, the cyclone is intensifying. Once the CDO, CF, and BF have all been taken into account, comparison of the imagery to the model can be accomplished. Figure 2 shows possible signatures of the tropical cyclone per designated T-number, and Figure 3 depicts actual images of tropical cyclones at each level. Note: not all tropical cyclones match exactly to what is depicted in Figure 2, however an overall “best fit” should be applied.

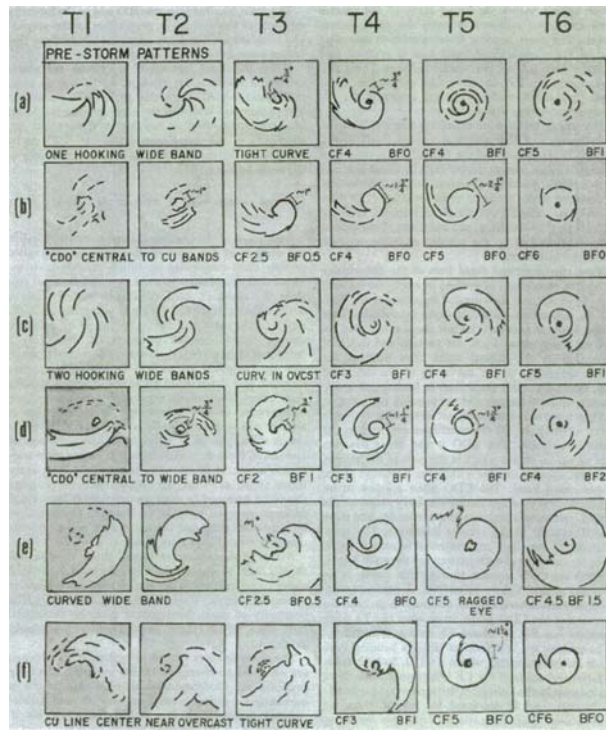


Figure 2. Common TC patterns and corresponding T-numbers (from Dvorak 1974 and used with permission of the AMS).

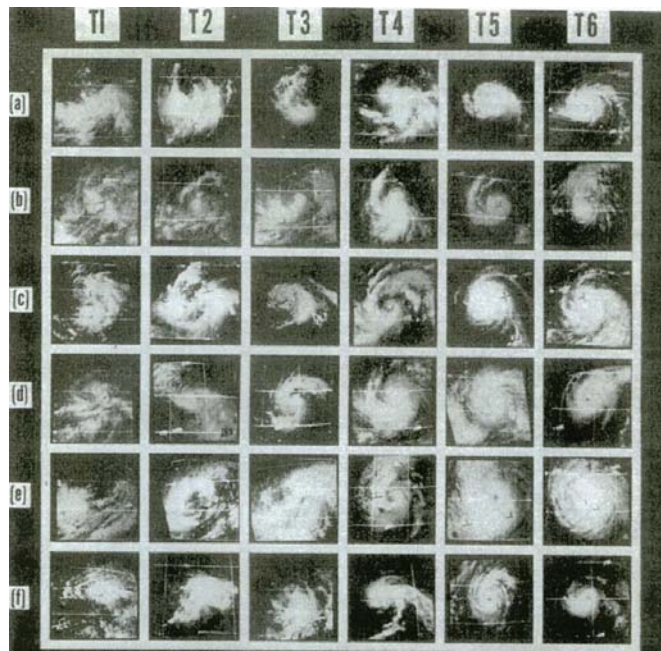


Figure 3. Examples of TC patterns (from Dvorak 1974 and used with permission of the AMS).

This method, based on pattern recognition, is used when the CDO obscures the exact center of the cyclone or the low-level cyclonic rotation is not easily identified. Streamlines can also aid in determining the overall circulation of the TC center. A second way to calculate the T-number is by using a LOG10 spiral graph.

The LOG10 method is employed in the event that the typhoon eye is clear and the BF and CF wrap well into the cyclone center. A resizable LOG10 spiral graph is overlaid on top of a visual or infrared satellite image of a tropical cyclone, keeping the spiral along the cloud shield major axis and relatively parallel to the inside region of the BF. Once there is a “best fit,” the analyst counts up the number of triangular sectors (each comprising 0.10) that the banding features encompass. The number of sectors is then compared to a reference corresponding to a sector count. Figure 4 depicts a LOG10 spiral graph, and Figure 5 shows the accompanying reference. The corresponding T-number determines how intense the tropical cyclone has become. In this particular example, the sector count is 0.85 and the T-number is 3.5 (McNamara 2001).

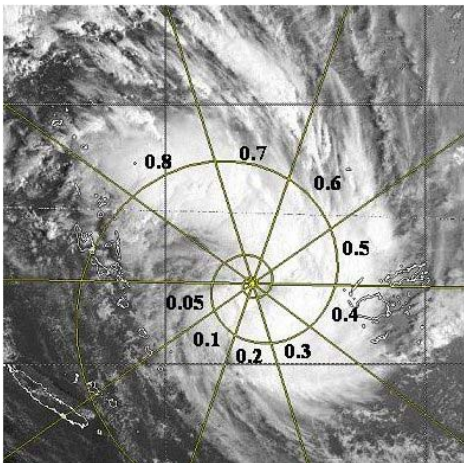


Figure 4. Example of a LOG10 spiral graph (modified from McNamara 2001 and used with permission of author).

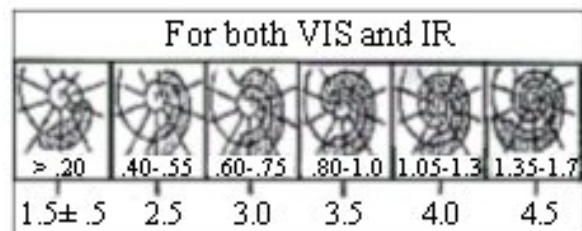


Figure 5. Corresponding LOG10 spiral graph reference (modified from McNamara 2001 and used with permission of author).



The objective of the pattern recognition and LOG10 methods is to compare today's imagery with yesterday's imagery to see how the cloud features have changed. If there is a good match with the T-number from yesterday's forecast, then there is high confidence in future intensification (given current rates of TC growth). If the comparison is not good based on the new imagery, then the T-number is adjusted for the new forecast. Finally, the last parameter the forecaster needs to calculate is the current intensity (CI) number.

“The CI number relates directly to the intensity of the cyclone (in terms of wind speed) for all typhoon events” (Dvorak 1974). The CI number is the same as the T-number during development, but remains higher during weakening (McNamara 2001). This rationale is based on the fact that storm surface vorticity is conserved even though cloud features are dissipating; the storm still has enough kinetic energy to fuel strong surface winds (McNamara 2001). Also, the CI number is maintained within  $\leq 1.0$  of the T-number during any phase. Table 1 shows the relationship between CI and the maximum wind speed (MWS) as well as minimum sea level pressure (MSLP).

The current intensity number along with the T-number provides a useful analysis of current tropical cyclone strength. These parameters are relayed to the public via a warning bulletin which also maintains continuity of typhoon strength between forecast shifts. Another useful measure of TC intensification is recognition of channel outflow patterns.

Table 1. Empirical relationship between CI number and MWS, and the relationship between the T-number and MSLP (modified from Dvorak 1974 and used with permission by the AMS).

C.I. Number	MWS (knots)	T Number	MSLP (mb) (Atlantic)	MSLP (mb) (NW Pacific)
1.0	25	1.0		
1.5	25	1.5		
2.0	30	2.0	1009	1003
2.5	35	2.5	1005	999
3.0	45	3.0	1000	994
3.5	55	3.5	994	988
4.0	65	4.0	987	981
4.5	77	4.5	979	973
5.0	90	5.0	970	964
5.5	102	5.5	960	954
6.0	115	6.0	948	942
6.5	127	6.5	935	929
7.0	140	7.0	921	915
7.5	155	7.5	906	900
8.0	170	8.0	890	884

## *2.2 Channel Outflow Patterns and Opposite Hemisphere Effects*

During the year long period of the First Global Atlantic Research Project Global Experiment (FGGE), Gray and Chen, Colorado State University researchers, studied upper tropospheric outflow patterns and correlated intensification and weakening based on those patterns. Intensifying tropical cyclones within the different global ocean basins typically showed upper level outflow patterns of three basic types: single channel outflow (S) which included either poleward or equatorward outflow; double channel outflow (D) in both poleward and equatorial directions; or no channel outflow (N) (Chen and Gray 1985). Each category of channeling was subcategorized by position of the

cyclone center to the outflow. For example, a tropical cyclone centered west of a single channel poleward outflow would be designated  $S_{PW}$  while a tropical cyclone centered underneath a double outflow channel would be designated  $D_C$ . Figure 6 shows a matrix of different cyclone centers and corresponding channels.

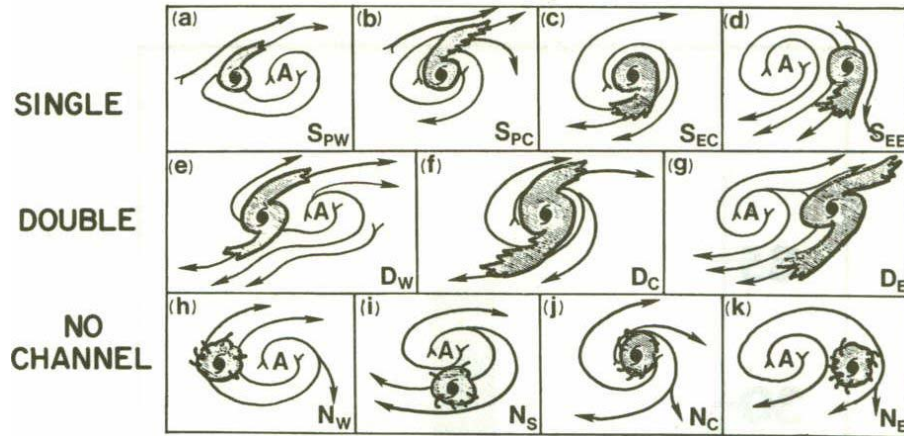


Figure 6. Variety of outflow patterns associated with TC intensification for Northern Hemisphere cases (from Chen and Gray 1985 and used with permission of author).

Chen and Gray studied numerous tropical cyclone events, and an analysis of maximum sustained winds verified the hypotheses of intensification based on outflow channels. An outflow channel is a narrow region of high speed flow (usually at 200 mb or approximately 40,000 feet altitude) which evacuates air from the tropical cyclone center. It is this evacuation of air which allows convection to occur inside of the eyewall and operates as an exhaust mechanism for continued intensification. Outflow channels are readily apparent from satellite imagery as long bands of clouds streaking anticyclonically from the cyclone center. Chen and Gray (1985) found that double channel outflows were associated with the fastest intensification rates. For single channel

patterns, equatorial outflow channels on average lead to faster intensification rates than poleward channel outflows. Given the variety and location of typhoons within the database, a comparison was also made between opposite pressure and hemisphere effects on TC intensification.

Both the location and strength of anticyclones in each hemisphere determined intensification and weakening via connections with the outflow channels. For example, it was noted that a strong equatorial upper level anticyclone in the southern hemisphere (SH) was extremely favorable for enhancing the equatorward outflow of a northern hemisphere (NH) tropical cyclone and vice versa (Chen and Gray 1985). TD Judy rapidly intensified into Super Typhoon Judy (maximum winds 135 kts) between 17 and 20 August 1979, due to this positive feedback mechanism. In 1972, rapid deepening of typhoons Rita, Phyllis, and Tess was “associated with multi-directional outflow channels to the large-scale flows of the upper troposphere” (Sadler 1978). However, it was also found that when an upper level SH anticyclone weakened or moved out of proximity to a NH tropical cyclone, diminishing of the outflow channel would result in steady or rapid weakening. Sadler (1978) noted these effects with Typhoon Rita, located northwest of Guam. Between 11 and 14 July 1972, the loss of a strong outflow channel resulted in rapid filling (910 mb to approximately 965 mb). These examples show how the diversity of opposite hemisphere anticyclones can strengthen or weaken a typhoon. Although the literature does not specify the approximate distance from the equator, all of the figures in the paper suggest anticyclones are located within 15 degrees of the equator for the effect to occur.

Given the validity of these findings, it has become imperative for the forecaster to monitor cross equatorial effects as well as same hemisphere effects. It is the combination of a current analysis technique such as Dvorak with an opposite hemisphere relationship that can dictate future intensity for storms in the vicinity of the equator. However, these parameters alone should not be regarded as the only measures of intensification. Other dynamical features, such as potential vorticity, can also explain why a typhoon rapidly intensifies.

### *2.3 Potential Vorticity Superposition and Anomalies*

Many researchers have argued that the interaction of tropical cyclones with upper-tropospheric troughs lead to a weakening of the system, whereas others believe this interaction aids in intensification. In a study conducted on Tropical Cyclone Danny in 1985, Molinari et al. (1998) “maintain that potential vorticity (PV) has become a useful dynamical framework for examining the interactions of tropical cyclones and upper-tropospheric vorticity maxima.” In addition, Bluestein (1993) “uses Rossby’s potential vorticity  $P$ :

$$P = -g(\zeta_{\theta} + f) \frac{\partial \theta}{\partial p} \quad (1)$$

where

$$\zeta_{\theta} = \left( \frac{\partial v}{\partial x} - \frac{\partial u}{\partial y} \right)_{\theta} \quad (2)$$

and  $P$  is considered potential vorticity.”  $\zeta_\theta$  is defined as relative vorticity,  $g$  is gravity, and  $f$  is the Coriolis parameter. Bluestein (1993) found that for typical midlatitude, synoptic-scale flow

$$P \approx -gf \frac{\partial \theta}{\partial p} \quad (3)$$

and typically

$$\frac{\partial \theta}{\partial p} \approx -\frac{10K}{100mb} \quad (4)$$

where  $\frac{\partial \theta}{\partial p}$  represents the partial derivative of potential temperature with respect to

pressure. Therefore, isentropic potential vorticity is on the order of

$$P \approx -(10m s^{-2})(10^{-4} s^{-1}) \left( -\frac{10K}{10kPa} \right) \frac{1kPa}{10^3 kg m s^{-2} m^{-2}} = 10^{-6} m^2 s^{-1} K kg^{-1} \equiv 1PVU \quad (5)$$

which agrees with the potential vorticity unit (PVU) as defined by Hoskins et al. (1985).

The importance of converting into isentropic potential vorticity (IPV) “thinking” is that analyses are made easier when working with synoptic-level charts (i.e., orders of magnitude are diminished). Bluestein (1993) also states that “values less than approximately 1.5 PVU are usually associated with tropospheric air, while larger IPV values are typically associated with stratospheric air.” In the study involving TC Danny, Molinari et al. (1998) found that the cyclone experienced rapid pressure falls as a relatively small-scale, positive upper potential vorticity anomaly began to superpose with the low-level center. Although the details of exactly how this interaction worked remains unclear, it was proposed that a constructive interference process initiated an evaporation-wind feedback instability (“WISHE” mode; Emanuel 1986). WISHE is a Wind Induced

Surface Heat Exchange in which inflow generates evaporation of the water vapor in the eyewall and releases latent and sensible heat to the system.

Given the complex dynamics of IPV, Bluestein (1993), Thorpe (1986), and Hoskins et al. (1985) found that the wind field or components of the wind field could be computed based on the distribution of IPV. Therefore, if large values of upper-level IPV were superposed with a surface tropical cyclone, the effects would be similar to those of large values of wind shear. The tropical cyclone would not intensify and/or would weaken because of the unfavorable conditions (see discussion in Section 2.5.2). The optimal state for intensification occurs as the tropical cyclone interlocks with small values of IPV. A small superposition provides enough shear for development but not too much which would separate the upper and lower cyclone structure. This rationale agrees with the hypothesis of Molinari et al. (1998) given the relationship between upper level troughs and upper level vorticity maxima. The upper level trough can also be examined in terms of the tropical upper tropospheric trough, which is another mechanism of typhoon intensification.

#### *2.4 Tropical Upper Tropospheric Trough Interactions*

The TUTT is defined as “A semi permanent trough extending east-northeast to west-southwest from about 35°N in the eastern Pacific to about 15°-20°N in the central west Pacific” (Glickman et al. 2000). Sadler (1975) found that the TUTTs “appear in summer monthly averaged maps of upper-tropospheric flow over the oceans.” Therefore, for most practical purposes, tropical cyclone intensification should be at its maximum

extent between June and September. Many studies have been accomplished and determined that it is the interaction with this trough (or series of cold lows) which aids in the intensification of tropical cyclones. Similar to the interactions of PV anomalies, the origin of the TUTT remains somewhat of a mystery, given that it is not a permanent feature.

Ferreira and Schubert (1999) have noted that “in water vapor images and upper-level IPV plots, TUTT cells appear as dry regions (dark in the water vapor imagery) of intense cyclonic PV.” They propose that TUTT cells originate as extrusions of midlatitude stratospheric air into the tropics. This proposition agrees with the PV research by Molinari et al. (1998). Observational studies by Kelley and Mock (1982), Whitfield and Lyons (1992), and Price and Vaughan (1992), found that “TUTT cells are cold core cyclones whose typical horizontal scale is on the order of several hundred kilometers. They also found that TUTT cells typically last for less than five days but may, in some cases, persist for nearly two weeks.” An important relationship between TUTT cells and tropical cyclone intensification has been proximity to each other.

Previously, it was stated that an optimal distance to the TUTT existed for typhoons to intensify (given small values of IPV). This relationship also holds true for the horizontal distance to upper cyclones. The upper cyclone (UC) is generally observed at the 200 to 250 mb level, and Sadler (1978) found that, in particular, north to northwest of the tropical cyclone is the optimal position of the UC for efficient mass and heat evacuation. This process allows the outflow channel access to the midlatitude westerlies. Chen and Gray (1985) took this idea further and established six basic types of interactions between tropical cyclones and their environments. Figure 7 depicts



positioning of TUTTs or mid-latitude troughs and the development of different outflow channels.

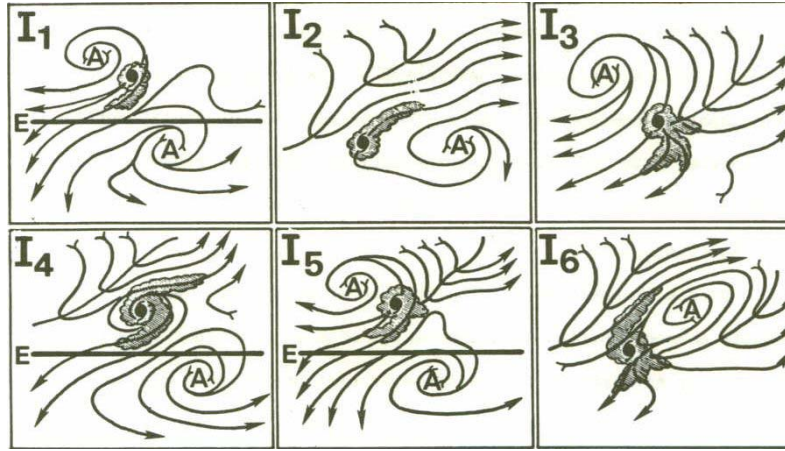


Figure 7. Six types of interactions between a TC and its surroundings (from Chen and Gray 1985 and used with permission of author).

The matrix in Figure 7 is based upon the following descriptions (Chen and Gray 1985):

I<sub>1</sub>: Equatorial anticyclone of the opposite hemisphere enhancing a single equatorward outflow channel.

I<sub>2</sub>: Long-wave middle latitude trough moving eastward to the poleward and west side of the cyclone so as to enhance a single poleward outflow channel.

I<sub>3</sub>: Tropical cyclone is located at the tip of or in the rear of a transverse long-wave trough (or TUTT). This arrangement acts to bring about the enhancement of a single equatorward outflow channel.

I<sub>4</sub>: Mid-latitude long-wave trough (or TUTT) and equatorial anticyclone of the opposite hemisphere approach a tropical cyclone from different directions and contribute to the establishment of double outflow channels in both poleward and equatorial directions.

I<sub>5</sub>: Combined effect of an equatorial anticyclone of the opposite hemisphere and the tip of a transverse upper shear line over the mid ocean enhancing a single equatorial outflow channel.

I<sub>6</sub>: Tropical cyclone flanked by western and eastern shear lines. This situation contributes to the establishment of double outflow channels.

Hanley et al. (2001) studied the interactions of tropical cyclones with upper-tropospheric troughs and classified trough interaction into four composites: (i) favorable superposition (tropical cyclone intensifies with an upper-tropospheric PV maximum within 400 km of the tropical cyclone center), (ii) unfavorable superposition, (iii) favorable distant interaction (upper PV maximum between 400 and 1000 km from the tropical cyclone center), and (iv) unfavorable distant interaction. In their study, they concluded that “78% of superposition and 61% of distant interaction cases deepened while undergoing a trough interaction” (given warm sea surface temperatures and distant proximity to land). And in the favorable superposition composite, intensification began soon after a small-scale upper-tropospheric PV maximum approached the storm center.

However, not all upper cyclones work toward the benefit of enhancing the strength and power of a tropical cyclone. In the event a UC crosses the path of or moves too close to a TC, the increase in vertical shear will tend to separate the upper-level anticyclonic outflow from the low-level cyclonic circulation. In addition, the UC which originally aided in outflow channel development can quickly extinguish this outflow. This weakening was the case with Typhoon Phyllis and Typhoon Tess in 1972 during the study composed by Sadler (1978).

As discussed in Section 2.2, it is incumbent upon the forecaster to maintain situational awareness. An environment which promotes positive feedback between the TUTT or upper cyclone can quickly change and cause rapid weakening. It is important to know the overall movement and juxtaposition of major pressure systems in order to correctly predict intensity changes. This knowledge can mean the difference between a rapid deepener and a typhoon which increases less than 1.0 T-number per day.

## *2.5 Environmental Influences*

*2.5.1 Sea Surface Temperatures.* One of the main, if not primary, sources of energy during the lifecycle of a tropical cyclone is sea surface temperature (SST). The ability of the typhoon to extract energy from the ocean's surface via latent heat release and sensible heat exchange dictates how powerful the cyclone can become and how quickly it can achieve its maximum potential intensity (MPI). Evans (1993) conducted a study based on the work of Merrill (1987) in five different ocean basins (North Atlantic, western North Pacific, South Pacific-Australian, northern and southern Indian Ocean) to determine the sensitivity of tropical cyclones to sea surface temperature. Merrill's research was based on the relationship between maximum surface wind speed and sea surface temperature. From his findings, he derived a "capping function" that was designed to portray the MPI of a storm for a given SST. Evans (1993) used this discovery to determine whether or not SST would be an adequate predictor of TC intensity. After analyzing storms in each of the basins and running statistical analyses of several TC events, Evans concluded that above a minimum threshold, SST does not seem to be the overriding factor in determining the maximum storm intensity. She cited that Merrill (1988) suggested many other possible influences, and it is probable that the synergistic effects on and above the ocean surface enable intensification to occur.

However, given the complexity of ocean heat exchange, it is important to note that tropical cyclones rarely develop in water cooler than 25°C (see also Holland 1997). In fact, many of the storms which move across cooler SSTs will undergo some form of weakening. On the other hand, storms which move across warm water eddies, such as

Hurricane Opal in 1995, can experience rapid intensification. In this particular event, Opal's sustained wind speed increased from 38 to 52 m s<sup>-1</sup> in 16 hours. Evans (1993) concluded "there is a hint, especially in the western North Pacific data, that some minimum SST threshold (~ 27°C) exists, above which the most intense storms occur." Holliday and Thompson (1979) proposed a necessary condition of 28°C SST for rapid intensification of typhoons, and Nyoumura and Yamashita (1984) found that typhoon intensification was more likely over warm water, particularly warmer than 28°C as well.

Although this was not the direct means of Hurricane Opal's intensification, in the Gulf of Mexico, as stated by Bosart et al. (2000), there was a correlation between the higher Gulf of Mexico SST and hurricane/tropical cyclone intensification events. As a final point of interest, Evans (1993) noted that "while SST will certainly influence tropical cyclone development, it is not the dominant factor in determining the instantaneous storm intensity nor the lifetime maximum intensity of the storm." It is probable that sea surface temperature plays a vital role in the rapid intensification or weakening of a typhoon. It is the combination of SST with other environmental factors, such as vertical shear, which needs to be taken into consideration for intensity forecasts.

*2.5.2 Effects of Vertical Shear.* Vertical shear is a change in the vertical wind profile, both in speed and/or direction and enables or disables the occurrence of convective development. Just as midlatitude thunderstorms require an exhaust mechanism to properly ventilate heat and mass, tropical cyclones employ a similar mechanism called "in-up-and-out." Moist inflow enters the eyewall region and through the WISHE process, provides an enhancement of cumulus (Cu) and cumulonimbus (Cb) development

within the spiraling rainbands. The “out” part is movement of air along the outflow channels which allows for continued inflow into the eyewall. Vertical shear enables the in-up-and-out process to work and plays an important role in TC intensification. If vertical shear is excessive, the lower region of the system will lose dynamic connections with the upper (outflow) regions, and the tropical cyclone will break apart. If vertical shear is too weak, there will not be enough ventilation of heat and mass to initiate new convection or maintain current levels of convection. In addition, the horizontal extent and location of the tropical cyclone also play a role in the effects of vertical shear.

During a large-scale analysis of Atlantic hurricanes, DeMaria (1996) found that high-latitude, large, and intense tropical cyclones all tend to be less sensitive to vertical shear effects than low-latitude, small, and weak storms. He defines high-latitude as systems located north of 29°N and low-latitude as systems located south of 20°N.

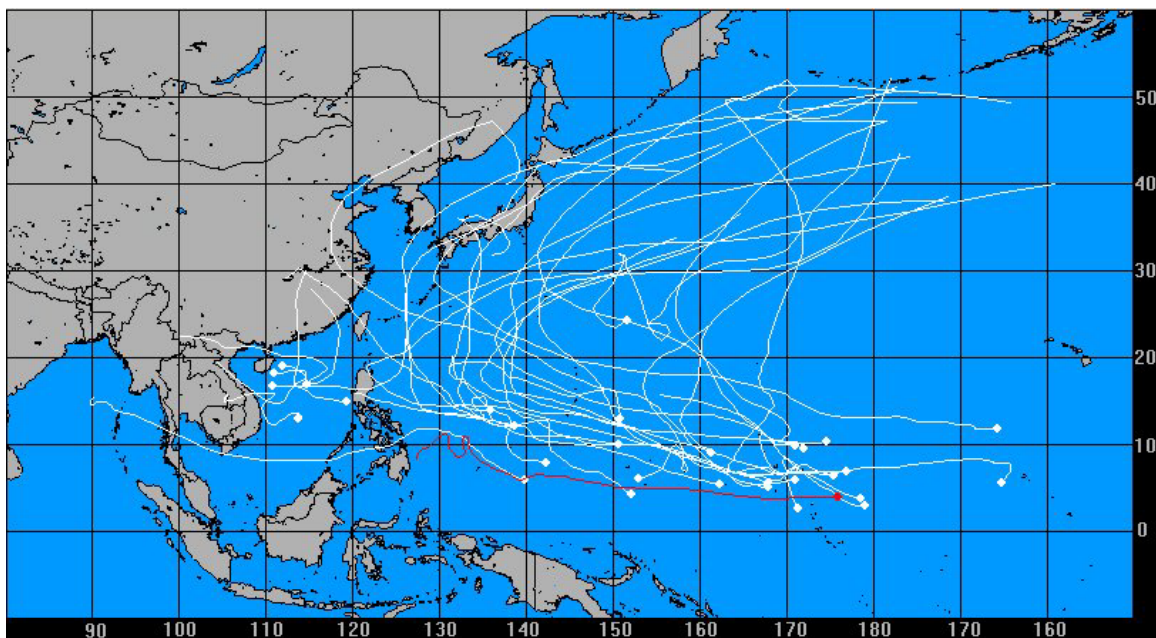


Figure 8. 1997 Northwest Pacific TC tracks (from the Global Tropical Cyclone Climatic Atlas 2003).

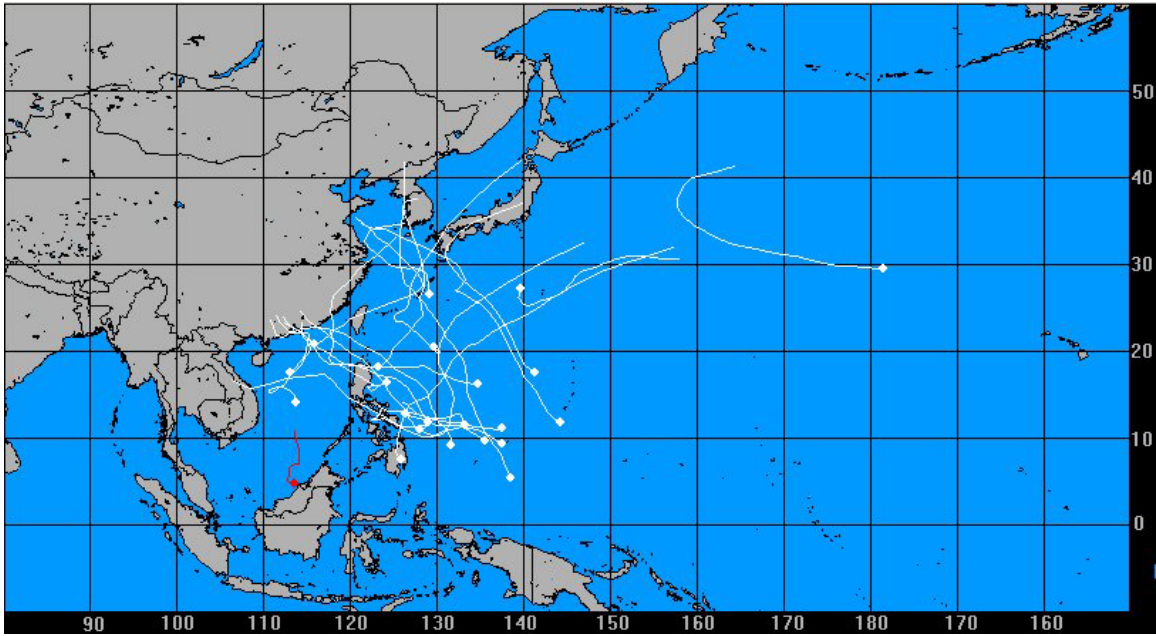


Figure 9. 1999 Northwest Pacific TC tracks (from the Global Tropical Cyclone Climatic Atlas 2003).

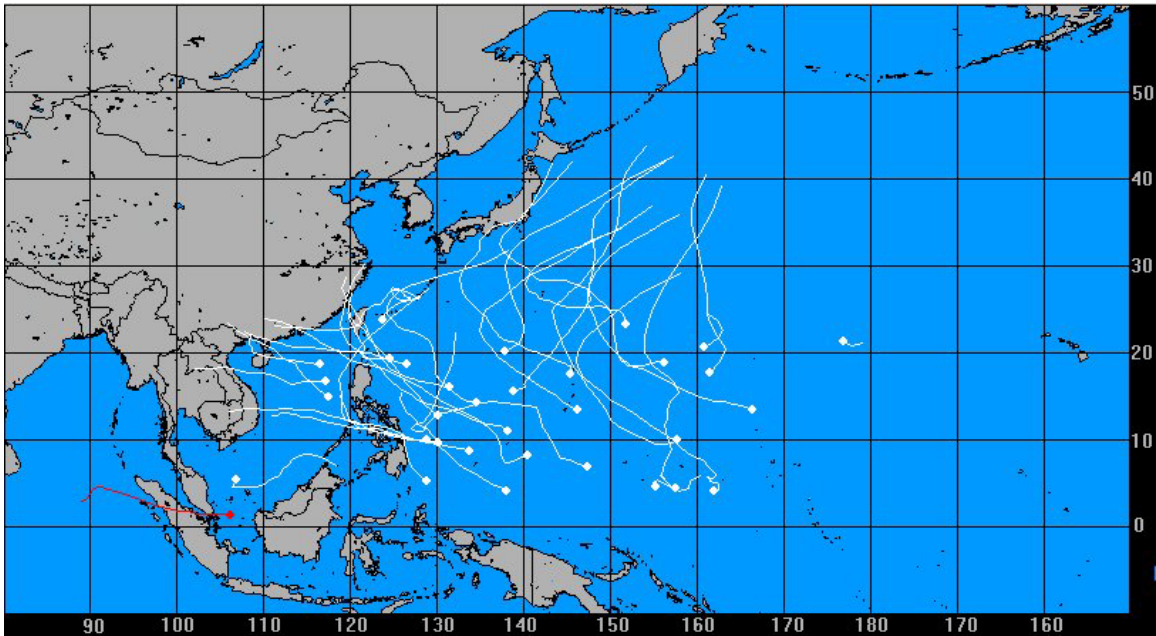


Figure 10. 2001 Northwest Pacific TC tracks (from the Global Tropical Cyclone Climatic Atlas 2003).

Figures 8 through 10 depict the tracks of northwestern Pacific Ocean tropical cyclones during 1997, 1999, and 2001. Based on the tightest grouping of tracks, it is easy to conclude that the majority of storms during the past several years fall under DeMaria's criteria of low latitude. Therefore, it is expected that given similar climatological conditions, future tropical cyclones will be sensitive to the effects of vertical shear. In addition, typhoons located north of about 30°N will be caught up in the mid-latitude westerlies, therefore becoming extratropical and weaken rapidly due to high shear.

For tropical cyclones located between 20°N and 29°N, DeMaria does not make specific reference as to the effects of vertical shear. Therefore, it is possible that the effects cannot be treated individually, but rather as a secondary or tertiary mechanism supporting an overall intensification or dissipation trend.

*2.5.3 Air-Sea Interactions.* The interactions between air and sea closely parallel the sea surface temperature discussion in Section 2.5.1. The main focus is the process by which the typhoon extracts energy from the boundary layer near the ocean surface. This is accomplished through high percentages of relative humidity (RH). RH unlocks a key to the development of the MPI through deep convection in the eyewall. As latent heat release occurs, larger percentages of RH provide needed water vapor, and Cb towers grow higher into the troposphere, enhancing the overall strength of the TC.

Holland (1997) found that a “derived MPI is highly sensitive to the surface RH under the eyewall, to the height of the warm core, and to transient changes of SST.” The limitations on how high the eyewall can develop stem from the availability of moist entropy between the ocean surface and the base of the clouds. Here, Holland defines

moist entropy as equivalent potential temperature,  $\theta_E$ , which is a function of pressure and temperature. As the tropical cyclone's central pressure lowers during constant or relatively constant SST,  $\theta_E$  increases. This process develops a positive feedback mechanism which in turn lowers the surface pressure. Therefore, as long as the central pressure is able to decrease, the TC should intensify. However, there is a limitation to the amount of energy the storm can extract, which is primarily based on overall movement. Storms which stagnate can undergo weakening even while they continually feed off of the ocean water vapor via evaporation and latent heat release.

Evaporation of water vapor from the ocean surface is a cooling process and will begin to lower the SST over time. This effect is not as drastic as upwelling, but it has been shown that tropical cyclones which move across waters previously occupied by a system do not have access to the same degree of surface temperature (i.e., moist entropy). The wake of a tropical cyclone leaves cooler surface waters, and consequently can decrease the amount of intensification of a subsequent TC via cooler inflow (see also Black and Shay 1998). In a similar study, Sikora et al. (1976) found that “measuring 700 mb  $\theta_E$  is a useful way to measure the total thermodynamic energy because it accounts for both latent and sensible heat. Their study parallels the work done by Holland (1997) by correlating minimum central surface pressure to 700 mb  $\theta_E$ .”

## *2.6 Upper Tropospheric Flow Transitions*

Upper tropospheric flow transitions (UTFT) provide an alternate means of intensification by enabling tropical cyclones to intensify without explicitly relying upon a



change of conditions at the surface. In particular, UTFT usually change the environmental winds which make access to outflow channels more conducive. This process is accomplished via relaxation of a major upper-level trough west of the tropical cyclone as anticyclogenesis occurs near the equatorward edge of the trough (Davidson and Kar 2002). As relaxation occurs, large-scale vertical shear is also reduced, allowing for more vigorous convection to develop within the eyewall. A “new” trough develops downstream of the TC and opens up access to the midlatitude westerlies and tropical easterlies. This outflow provides even further intensification by increasing the ventilation of heat and mass from the cyclone core. However, if the typhoon eye begins to migrate into the westerlies, increased shear will induce weakening.

Davidson and Kar (2002) as well as Chen and Gray (1985) found that rapid intensification may occur once access to these upper level outflow channels has been established. In addition, upper level cyclonic circulation is enhanced, which leads to the onset of more moist, deep convection. Sadler (1978) also showed that intensification was favorable as the tropical cyclone moved into optimum proximity with the UC. This rationale is also consistent with the PV superposition and anomalies suggested by Molinari et al. (1998). Even though UTFT cannot be treated individually, as a mechanism for TC intensification, they play an integral part of the overall dynamics. Coupled with outflow channel access and PV superposition, UTFT provide useful insight into the synoptic patterns at 200 mb which can lead to explosive intensification. Understanding upper tropospheric flow transitions, as well as TUTT interactions and channel outflow patterns, provide better awareness in forecasting tropical cyclone intensity changes.

### **III. Methodology**

#### *3.1 Introduction*

The overall goal of this research is to data mine atmospheric parameters responsible for typhoon rapid intensification and weakening and to validate the usefulness of using these parameters in the forecast process. These predictors vary from environmental conditions (such as sea surface temperature) to model derived fields (such as wind shear). Currently, JTWC only uses the Dvorak Technique to forecast intensification trends, and the objective of this research is to broaden the tools used in these forecasts. In order to meet this expectation, CART data mining is used to develop the new tools. This analysis employs various splitting rules (discussed further in Section 3.3.1), combined with both simple linear regression and classification analysis techniques.

#### *3.2 Data Acquisition*

*3.2.1 Storm Selection.* As mentioned in Section 1.2, using typhoons from different climatological regimes (EN, LN, NU) is important. These regimes serve as yet another predictor in supporting or inhibiting rapid intensification. Of the total number of tropical events in 1997, 1999, and 2001, 27 storms are selected for research since specific criteria needed to be met. These 27 storms are all typhoon strength or greater and exhibit some form of rapid intensification or rapid weakening during their lifecycle. The criteria for

this determination is a change in winds  $\geq 50$  kts per 24 hours and/or a change in pressure  $\geq 15$  mb per 6 hours (JWTC Website TDO Handbook 2003). Table 2 lists storms which meet this criteria, where T refers to typhoon and ST refers to super typhoon.

Table 2. Selected typhoons from 1997, 1999, and 2001.

1997 - El Nino	1999 - La Nina	2001 - Neutral
02C ST Oliwa	05W T Leo	04W T Chebi
05C ST Paka	06W T Maggie	06W T Utor
07W ST Nestor	16W T Sam	10W T Yutu
10W ST Rosie	24W ST Bart	11W T Toraji
17W T Zita	26W T Dan	12W T Man-Yi
18W T Amber		16W ST Wutip
24W ST Ginger		20W T Nari
27W ST Ivan		23W T Lekima
28W ST Joan		24W T Krosa
29W ST Keith		26W ST Podul
		27W T Lingling
		33W ST Faxai

*3.2.2 Best Track Data.* The best track (BT) data set serves as the official record (nearest ground truth) of a typhoon's progress. It is a six-hourly fix of each storm including latitude/longitude, maximum sustained wind speed (kts), and minimum sea level pressure (mb). The data set is obtained from the JTWC webpage, which is available online at [http://www.npmoc.navy.mil/jtwc/best\\_tracks/](http://www.npmoc.navy.mil/jtwc/best_tracks/), as well as the Global Tropical Cyclone Climatic Atlas (GTCCA) (<http://navy.ncdc.noaa.gov/products/gtcca/gtccamain.html>). In addition, a complete description of extra parameters, not always included in the data, can be found from JTWC ([http://www.npmoc.navy.mil/jtwc/best\\_tracks/wpindex.html](http://www.npmoc.navy.mil/jtwc/best_tracks/wpindex.html)).

Table 3 is a sample of what BT data would look like from the GTCCA webpage.

Table 3. Sample best track data for TC 04 (modified from the Global Tropical Cyclone Climatic Atlas 2003).

Year	Month	Day	Hour	Lat	Lon	Spd	Dir	Max Wnd	Min Pressure
2001	06	19	06	11.1	138.4	99.9	999	020	1004
2001	06	19	12	11.7	137.5	99.9	999	025	1002
2001	06	19	18	11.8	135.9	99.9	999	030	1000
2001	06	20	00	12.3	134.5	99.9	999	030	1000
2001	06	20	06	13.0	133.1	99.9	999	035	0998
2001	06	20	12	13.7	131.4	99.9	999	040	0994
2001	06	20	18	14.1	129.2	99.9	999	045	0991
2001	06	21	00	14.6	127.9	99.9	999	045	0991
2001	06	21	06	15.2	127.2	99.9	999	050	0991
2001	06	21	12	16.0	125.9	99.9	999	055	0984
2001	06	21	18	17.1	124.7	99.9	999	060	0980
2001	06	22	00	18.3	123.6	99.9	999	065	0976
2001	06	22	06	19.3	122.4	99.9	999	075	0967
2001	06	22	12	20.3	121.1	99.9	999	075	0967
2001	06	22	18	21.1	119.9	99.9	999	090	0954
2001	06	23	00	22.1	119.4	99.9	999	100	0944
2001	06	23	06	23.3	119.1	99.9	999	095	0949
2001	06	23	12	24.8	119.4	99.9	999	090	0954
2001	06	23	18	26.3	119.7	99.9	999	085	0954
2001	06	24	00	28.3	120.5	99.9	999	045	0991
2001	06	24	06	30.1	121.9	99.9	999	035	0997

*3.2.3 NOGAPS Model.* As discussed in Section 1.2, the NOGAPS model serves as the primary source of model data in this research for the Pacific basin. It is a global model (spectral in the horizontal) and is available at six-hourly intervals which correspond well to the BT data. Archived NOGAPS analyses are obtained from the FLENUMMETOC Detachment at AFCCC. The model is currently output on a 1 x 1 degree grid (archived on a 2.5 x 2.5 degree grid), and only the western North Pacific regions are used.

NOGAPS uses conventional observations for the analysis and relies heavily on satellite soundings and derived wind fields. The data set coverage for the 27 storms extends from

5°N to 47.5°N latitude and from 165°W to 100°E longitude. One initial and very important consideration in using this model data with ~ 150 nm between grid points, is to most closely match the typhoon center to the nearest latitude and longitude of the model domain. In order to accomplish this task, a MATLAB program is written to associate the typhoon to the nearest grid point. This technique assumes a certain margin of error since the maximum distance could be as large as 106 nm if the core is exactly between grid points. However, since no other available model provides the needed coverage, this potential error is noted during the collection of the model fields. Table 4 lists the different model fields used in this research

Table 4. NOGAPS model fields.

Level	Model Fields
Surface	T, RH, U, V
1000 mb	T, RH, U, V
850 mb	T, RH, U, V
200 mb	T, U, V

where T is temperature, RH is relative humidity, U is the east-west wind component, and V is the north-south wind component. In addition to the normally computed fields provided by AFCCC, another MATLAB program is created to calculate surface-200 mb, 1000-200 mb, and 850-200 mb wind speed and directional shear as well as surface, 1000 mb, 850 mb, and 200 mb winds. A complete listing of both MATLAB programs is found in Appendices A and B.

It is also important to note that some of the model data are unavailable during brief periods within the lifecycle of six typhoons. The storms which have missing data are listed in Table 5.

Table 5. Storms with missing model fields.

1997	2001
Paka (05C)	Chebi (04W)
Nestor (07W)	Man-Yi (12W)
	Wutip (16W)
	Nari (20W)

Although these storms are missing some data, they are still included in the overall analysis. By contrast, all of the selected storms in 1999 have a complete archive of the model fields.

*3.2.4 Sea Surface Temperatures.* Since the primary source of heat and energy required to sustain typhoon development is the ocean surface, SST data over the entire lifecycle of each typhoon are incorporated to the overall database. SSTs are also obtained from the FLENUMMETOC Detachment at AFCCC. These data are derived from the Air Force Weather Agency (AFWA) Surface Temperature (SFCTMP) Model. An in-depth discussion on the SFCTMP model is found in Kopp (1995), however the process is briefly discussed below.

For all water points in the SFCTMP Model, unchanged US Navy SST analyses are used. These analyses are received once daily, and each analysis is a global snapshot valid at 1200 Coordinated Universal Time (UTC). The US Navy collects SST values (from surface observations and satellite algorithms) which are mapped on a 0.25 x 0.25 degree grid, however the SFCTMP Model operates on a 0.125 x 0.125 degree grid. In order to populate the SFCTMP domain, a bilinear interpolation is used to remap the SST values to the proper grid spacing. In addition, the SST data are quality checked during

each model cycle. If any location over water has a temperature colder than 270 K or warmer than 310 K, that value is discarded, and the value from the previous cycle is used. “This procedure not only prevents unrealistic SSTs, but avoids an excessively noisy analysis” (Kopp 1995).

*3.2.5 CPC Teleconnection Indices.* The two teleconnection indices used in this research are the Southern Oscillation Index (SOI) and the Multivariate ENSO Index (MEI). The teleconnection indices are used to draw a relationship to EN, LN, and NU years. Both of these indices are obtained from the Climate Prediction Center (CPC) website (<http://www.cdc.noaa.gov/ClimateIndices/>) under the Niño 4 grid box, which is located between 5°N and 5°S latitude and between 150°W to 160°E longitude. A description of the standardized SOI can be found in Randall (2002). In essence, the SOI is the difference in the standardized anomalies of sea level pressure between Darwin, Australia and the Pacific Island of Tahiti (D’Aleo and Grube 2002, Ford 2000). Generally, a positive value of SOI is associated with EN phases, and a negative value is associated with LN phases. In addition to the SOI, a newly developed multivariate index is also used.

The MEI was developed to provide a new comprehensive data set that incorporates multiple factors, including air temperatures, sea surface temperatures, sea level pressure, surface wind, and cloudiness (D’Aleo and Grube 2002). Although the MEI does not provide coverage on a monthly basis, as the SOI does, it was developed in anticipation of becoming a new standard for measuring climatic changes. The MEI is measured on a bi-monthly basis (where the January value is the December-January

timeframe and the value is centered between the two months). D'Aleo and Grube (2002) suggest that significant ENs have MEIs  $> 1$  while significant LNs have MEIs  $< -1$ . Values of MEI between -1 and 1 are assumed to incorporate NU regimes, although the literature did not make specific reference to these values. CPC also maintains other various teleconnection indices, however the SOI and MEI are the only two deemed useful in this research. It is significant to note that there is some inherent error in using the Niño 4 grid box due to its location in the Pacific Ocean.

The majority of the typhoons originate near the international date line, however they propagate well past the western most edge of the grid box (which remains stationary regardless of the climatic regime). Therefore, some of the lifecycle is not covered by the index. In addition, due to the Coriolis force, tropical cyclones are not usually observed within 5 degrees north or south latitude of the equator. Thus, none of the storms are located under the northern most edge of the Niño 4 grid box. However, given the availability of climatic information and the association to tropical cyclones, SOI and MEI values are assumed to be representative of the entire lifecycle of the storm.

### *3.3 CART Overview*

Classification and regression tree analysis was developed in the early 1980s and has become one of the primary drivers in data mining research. The overall objective is to use decision trees in mapping a target variable (dependent response) from a set of predictors (independent variables). Classification and regression analyses both use decision trees, however only the classification analysis is considered important to this



research. This scheme utilizes a binary, recursive partitioning, tree growing algorithm which was developed by Breiman et al. (1984).

The classification approach uses a non-parametric statistical analysis which begins with the parent node. The data are divided into one of two child nodes according to a “yes” response (i.e., meets the splitting rule condition, discussed further in Section 3.3.1.1) or a “no” response (i.e., does not meet the splitting rule condition). Benz (2003) provides a detailed example of meeting splitting rule conditions. In order for the parent node to be split into two purer child nodes where purer refers to improved homogeneity of the data, the target variable must be categorical (e.g., A, B, C or 1, 2, 3). If the target variable contains discrete data, it is necessary to define these data as categorical variables (or “dummy” variables). The remaining predictors can also be defined categorically or retain their original values. Once the target variable has the correct format, the decision tree building process begins.

CART continues to split each subsequent child node until the optimal terminal node is reached, and it considers all possible splits for each of the predictors in the data set. The total number of splits is determined by the product of the predictors and number of records in the data set. For example, if there are 10 different predictors and 100 records of data, CART will consider 1000 different splits in formulating the optimal tree. A complete treatment of terminal node calculation is found in Breiman et al. (1984). After the full tree is grown, CART displays the optimal tree, showing the best splits based on the target variable. If it is undesirable to define the target variable categorically, then the regression method needs to be employed.

The CART regression scheme does not require a categorical target variable, however the only splitting rule used is least squares (discussed further in Section 3.4). Similar to the classification scheme, a regression analysis also creates a decision tree from which inferences about the partitioned data may be made.

### *3.3.1 Methods*

*3.3.1.1 Tree Splitting Methods.* In the classification analysis, there are six different splitting functions. Only two, Gini and Twoing, are employed for this research due to time constraints. The Gini function seeks to isolate the largest subset of data from the remaining population such that the largest group is placed in one child node and the rest in the other child node. For example, consider a data set with the following classified population (and quantity listed in parentheses): A (40), B (30), C (20), D (10). The Gini function would review the population of 100 and distribute Class A into one child node while Classes B, C, and D would go to the other child node. Then, at the second splitting level in the tree, Gini would distribute Class B into one child node, leaving Classes C and D in the other node. Finally, the third splitting level would result in one terminal node containing Class C and the remaining terminal node containing Class D. In total, there would be four terminal nodes, each with the highest level of homogeneity (see Figure 11 for a graphical look at this process).

The Twoing function operates in a similar fashion, however it attempts to isolate the same quantity of data among the child nodes. In Figure 12, notice that since the total sample space between Classes A and D (50) is the same as Classes B and C (50), Twoing

will separate Classes A and D into one child node, with Classes B and C into the other node. Then at the second split, each subset gets distributed into its own terminal node.

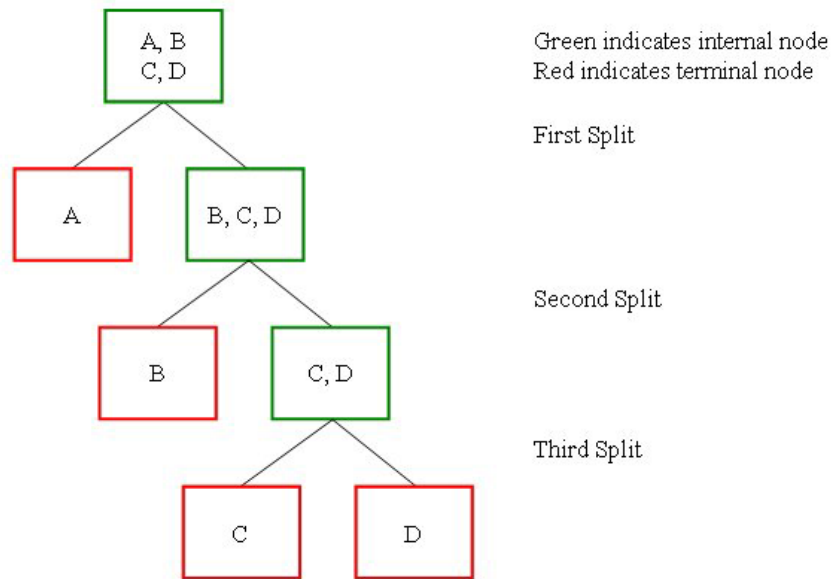


Figure 11. Sample Gini splitting function.

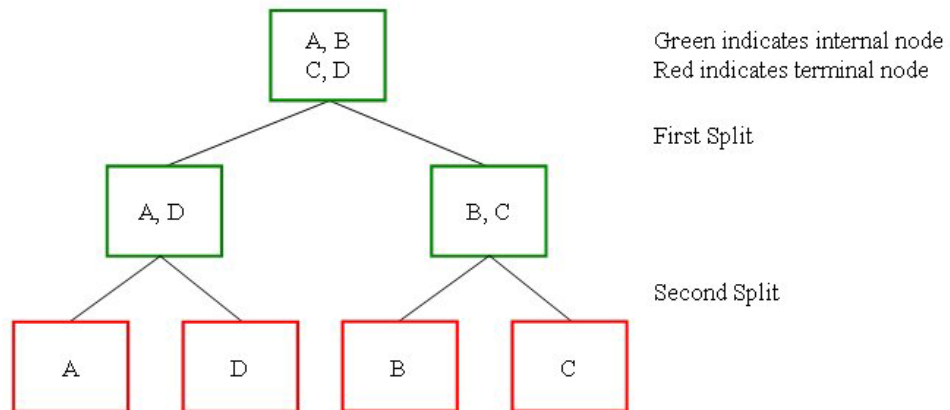


Figure 12. Sample Twoing splitting function.

If the population does not consist of perfect splits (i.e., 50-50), as illustrated in this example, the Twoing function will attempt to make the best split where 1/2 of the data is in each child node. In order to understand each splitting function, a brief description is given below.

The mathematical expression for the Gini function is given by

$$\sum_{j \neq i} p(i|t) p(j|t) \quad (6)$$

where  $p(i|t)$  is the probability of an object selected at random being distributed into Class  $i$  given Class  $t$ , and  $p(j|t)$  is the probability of an object selected at random being distributed into Class  $j$  given Class  $t$ . In Gini, “the impurity (or lack of homogeneity) is calculated by subtracting the sum of squared probabilities of each class within the given node summed over all levels of the categorical variable” (Steinberg and Colla 1995). This function is best thought of as peeling the layers (of an onion, for example) in order to isolate each subclass.

The mathematical expression for the Twoing function is given by

$$\frac{p_L p_R}{4} \left[ \sum_j |p(j|t_L) - p(j|t_R)| \right]^2 \quad (7)$$

where  $p(j|t_L)$  is the probability of an object being distributed into Class  $j$  given a left terminal node, and  $p(j|t_R)$  is the probability of an object being distributed into Class  $j$  given a right terminal node (Breiman et al. 1984). In Twoing, “the objective is to make the likelihood that a given class goes to the left as different as possible from the probability that it goes to the right” (Benz 2003). Furthermore, Equation 7 is maximized

when  $p_L$  and  $p_R$  each equal 0.5. Both splitting functions result in the same four terminal nodes (each containing an individual sample space), however the process in deriving the terminal nodes varies slightly. Breiman et al. (1984) did note that twoing the data gives “strategic” splits and informs the user of class similarities. Twoing is accomplished by grouping together large numbers of classes which have similar characteristics.

*3.3.1.2 Pruning.* The tree will continue to grow (splitting child nodes) until it is no longer able to split or until a pre-defined node size is reached. At this terminal node junction, the tree is at its largest size. There may, however, be nodes which can be removed (pruned) to improve the overall effectiveness of interpreting the outcome. For example, CART will remove nodes when each child has the same classification (such as Class A). This pruning is meaningful because the overall purpose is to achieve node purity by “complete” homogeneity within the node. Having two child nodes with the same class assignment does not provide more information than examining the parent node. In addition, CART will prune where the gain in improvement score (see Section 3.3.1.4) exceeds the loss in homogeneity. Breiman et al. (1984) suggest letting the tree grow to a maximum (i.e., splitting until the terminal nodes contain the smallest allowable node size), however this outcome may result in hundreds of terminal nodes. In this way, the interpretation becomes impractical, and the nodes need to be collected back toward the parent node. This process is called upward pruning, and CART will display each phase of the splitting process (allowing the user to manually upward prune at each level to examine the effects).

*3.3.1.3 Cross Validation.* If the data set is large enough (i.e., thousands of records), the user can divide the data into a learn sample and a test sample for validation of the final tree. However, in this research, the data set is too small to employ the learn and test sample procedure, therefore a 10-fold cross validation technique is used. According to Steinberg and Colla (1995), “the core idea of cross validation is that each observation is included in both the test sample and the learning sample.” The tree is grown for the first time using all of the data in order to provide an error rate reference. In 10-fold cross validation, the data are divided into approximately 10 equal and random subsets, and the process of growing the trees is repeated 10 separate times from the beginning. In each stage of cross-validation, nine subsets of the data are used to build the model (learn data), and one subset is used for testing. For each stage of testing, a different subset of the data is used whereas the same subset is not used twice. Also, the error rates are computed for each tree during that step in the sequence. When the 10 cycles are complete, the error rates from all 10 samples are summed in order to provide the overall error of the tree.

This method is appealing because once an observation is used for building the model, it is not available for testing and thus it does not influence the growth of the tree during that stage. Also, since every observation is used exactly once while the tree is being built, it has an equal probability of being correctly or incorrectly classified. Therefore, the total misclassification rates are correct for the complete data set (Steinberg and Colla 1995). Figure 13 shows a graphical look at the 10-fold cross validation process.

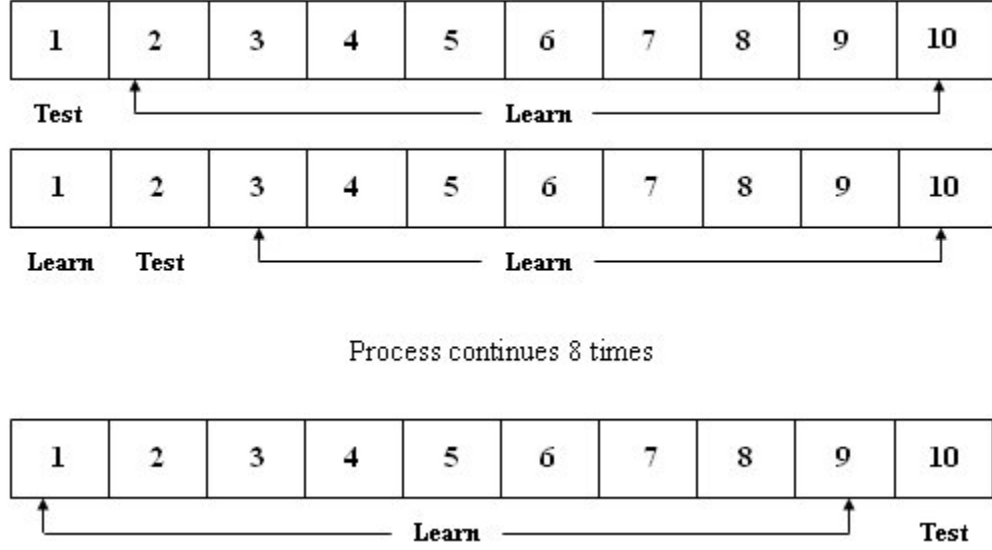


Figure 13. Graphical depiction of 10-fold cross validation (modified from Salford Systems 1995).

**3.3.1.4 Improvement Scores.** As each parent node splits, the assumption is that each child node has less impurity (i.e., more homogeneity in the data) than the parent. In building the optimal tree, CART measures the decrease in impurity from node to node, and this overall value is called the improvement score. Breiman et al. (1984) state that the improvement score is calculated by subtracting the sums of the child node impurities, multiplied by each respective probability of a left or right node distribution, from the parent node impurity. Figure 14 shows a graphical depiction of the split and resulting impurities. The equation of the improvement score after the split is given by

$$score = I_P - (I_L (prob_L) + I_R (prob_R)) \quad (8)$$

where *score* is the improvement score,  $I_P$  is the parent node impurity,  $I_L$  is the left child node impurity,  $prob_L$  is the probability of distributing to the left child node,  $I_R$  is the right child node impurity, and  $prob_R$  is the probability of distributing to the right child node.

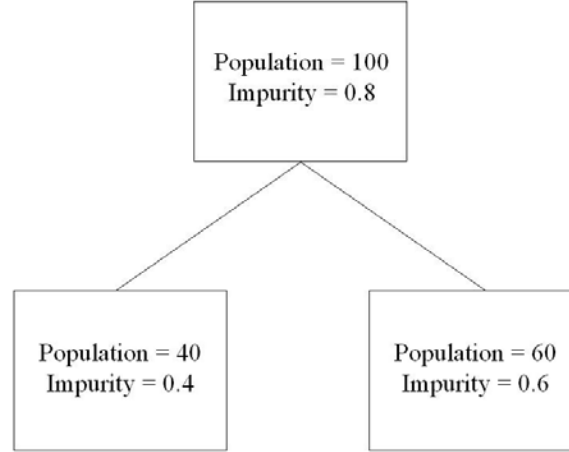


Figure 14. Example of an improvement score.

The improvement score in this example is  $0.8 - \left( 0.4 \left( \frac{40}{100} \right) + 0.6 \left( \frac{60}{100} \right) \right) = 0.28$ . Each time there is a split, an improvement score is calculated, and this score measures how well the split improves the predictive performance of the tree.

*3.3.1.5 Class Assignments.* One of the most important elements in assessing the overall quality of the classification tree is the percent error misclassification. The percent error misclassification stems directly from the class assignment in each terminal node, which is computed with Bayes' Theorem (Montgomery and Runger 2002). Equation 9 is used to determine the probability of a record going into a left child node ( $L$ ), given it is of Class  $n$

$$p(n_0 | L) = \frac{p(L | n_0) p(n_0)}{p(L | n_0) p(n_0) + p(L | n_1) p(n_1) + p(L | n_2) p(n_2)} \quad (9)$$

where  $n_x$  is Classes 0, 1, and 2. The individual probabilities,  $p(L | n_x)$  and  $p(n_x)$ , can be determined by two different means. When Priors Data is used, the probability of Class  $n$  is computed as the number of records in Class  $n$  divided by the sum of records (across



all classes) in that node. Priors Data states that the probability of each class is equal to the distribution of the class in the sample. When Priors Equal is used, the probability of Class  $n$  is exactly the inverse of the number of classes. Priors Equal states that the probability of each class is equal, regardless of the frequency distribution. The following example illustrates Priors Equal probability where the distribution of cases is

	<u>Parent</u>	<u>Left</u>	<u>Right</u>
Class 0	1037	241	796
Class 1	74	50	24
Class 2	87	3	84

The within-node probabilities are calculated as

	<u>Left</u>	<u>Right</u>
Class 0	0.247	0.373
Class 1	<b>0.717</b>	0.158
Class 2	0.036	<b>0.469</b>

where the class assignment for the left node is Class 1, and the class assignment for the right node is Class 2. Thus, all of the records not of Class 1 (left node) and Class 2 (right node) are misclassified. The percent error misclassification is based on the summation of the misclassifications per class in each terminal node of the entire tree.

*3.3.2 Research Predictors.* In order to employ the data mining software, 41 different predictors are selected, ranging from continuous numerical values to categorical values. Table 6 shows a list of the predictors used in this research. It is important to note that the predictors in italics are defined categorically according to discussions in Chapter 2. The rules which govern the categories are shown in Table 7, and the values are listed in Table 8. CLIMO is also categorical to account for the climatic regime once the data is merged. However, it's not included in Tables 7 and 8 because of a lack of favorable and

Table 6. List of CART predictors.

Predictor	Definition
MONTH	Month of typhoon lifecycle
AGE	Age in 6 hour timeframes
LAT	Latitude
SFC T	Surface temperature
SFC RH	Surface relative humidity
SFC U	Surface u wind component
SFC V	Surface v wind component
SFC SPD	Surface wind speed
SFC DIR	Surface wind direction
THSN T	1000 mb temperature
THSN RH	1000 mb relative humidity
THSN U	1000 mb u wind component
THSN V	1000 mb v wind component
THSN SPD	1000 mb wind speed
THSN DIR	1000 mb wind direction
E50 T	850 mb temperature
E50 RH	850 mb relative humidity
E50 U	850 mb u wind component
E50 V	850 mb v wind component
E50 SPD	850 mb wind speed
E50 DIR	850 mb wind direction
TWO T	200 mb temperature
TWO U	200 mb u wind component
TWO V	200 mb v wind component
TWO SPD	200 mb wind speed
TWO DIR	200 mb wind direction
STSS	Surface-200 mb speed shear
TTSS	1000-200 mb speed shear
ETSS	850-200 mb speed shear
STDS	Surface-200 mb directional shear
TTDS	1000-200 mb directional shear
ETDS	850-200 mb directional shear
SST	Sea surface temperature
SOI	Southern Oscillation Index
MEI	Multivariate ENSO Index
<i>CLIMO</i>	<i>Climatic regime (EN, LN, NU)</i>
<i>CH OUT</i>	<i>Channel outflow</i>
<i>OHEMI</i>	<i>Opposite hemisphere effect</i>
<i>TUTT</i>	<i>Interaction with TUTT</i>
<i>CAT STSS</i>	<i>Categorical speed shear</i>
<i>CAT STDS</i>	<i>Categorical directional shear</i>

Table 7. Rules for categorical predictors.

Predictor	Favorable Criteria	Unfavorable Criteria
CH OUT	Double or single	None
OHEMI	Within 15 deg of equator	Outside 15 deg of equator
TUTT	Within 1000 km (10 deg)	Outside 1000 km (10 deg)
CAT STSS	Speed shear < 15 kts	Speed shear $\geq$ 15 kts
CAT STDS	Directional shear < 45 deg	Directional shear $\geq$ 45 deg

Table 8. Categorical values for predictor rules.

Predictor	Favorable Criteria	Unfavorable Criteria
CH OUT	2 (double) & 1 (single)	0
OHEMI	1	0
TUTT	1	0
CAT STSS	1	0
CAT STDS	1	0

unfavorable criteria. In addition, the target variable is defined categorically according to the criteria discussed in Section 3.2.1. Class 2 indicates rapid intensification, Class 1 indicates rapid weakening, and Class 0 indicates no rapid changes.

The subjective analysis of channel outflow (CH OUT) and TUTT is accomplished by noting favorable influence (i.e., presence of channel outflow and interaction with TUTT) in the IR satellite imagery archived from BOM. The opposite hemisphere (OHEMI) predictor is also determined by IR satellite imagery, however the resolution of the imagery makes the subjective call more difficult. The archived NCDC prognostic charts of 200 mb geopotential height (GPH) and winds supplement this examination. If no closed contour of 200 mb GPH or well-defined (i.e., winds greater than light and variable) circulation in the 200 mb wind field exists within 15 degrees of the equator, then OHEMI is deemed as not occurring. Special attention is paid to equatorward outflows since these features are highly indicative of OHEMI. A southern equatorial

ridge is observed to help enhance the equatorward outflow. In addition, it appears that OHEMI effects were more influential to western Pacific events than events in the central Pacific. This observation might certainly be a factor when considering climatic regimes because EN years tend to show typhoon development further east and south whereas LN years tend to show typhoon development further west.

Initial rapid intensification almost always occurs when CH OUT is established 6 to 12 hours earlier. The dissipation of CH OUT (change in predictor category) is not specifically addressed in the literature, therefore it is assumed no longer occurring when a typhoon loses the majority of its characteristics (eye and symmetry) and/or is sheared by mid-latitude westerly flow. For storms which follow an extratropical path, mid-latitude flow usually affects the last 24 to 36 hours of their lifecycle.

The TUTT, which is a transient feature, is reserved exclusively for influences by the 200 mb trough in the central Pacific, although there are some instances of interactions with major shortwave troughs over eastern Asia and the western Pacific. These interactions are usually picked up by channel outflows, therefore they are not counted twice. If these trough effects don't have channel outflows occurring at the same time, they are not counted at all in the analysis. It is also noted that there are no TUTT influences during LN events. This lack of occurrence is most likely due to the fact that typhoons originate too far west in the Pacific, and they remain outside of an optimal north-northwest interlocking position to the upper trough during the course of their lifecycle.

Even though some of the predictors, such as STSS, STDS, and SST already have predefined intensification or weakening criteria, they are still included in the analyses. In

addition, categorical values of STSS and STDS are included to examine any differences from the actual values of speed and directional shear. These variables are included to validate the current rules-of-thumb and to see if JTWC guidelines change based on the three year data set. The predictors without predefined rules-of-thumb are data mined to determine relationships, if any, with the target variable. Predictors which are found conducive to typhoon rapid intensification or rapid weakening thus become the focus for deeper CART analyses and are discussed further in later chapters.

### *3.4 Statistical Overview*

*3.4.1 Introduction.* Regression analysis is used to explore the relationships between two or more variables. This examination is accomplished with simple linear regression (one predictor, an independent variable such as  $X$  and one response, a dependent variable such as  $Y$ ) or multiple linear regression (several predictors such as  $X_1, X_2, \dots, X_n$  and one response such as  $Y$ ). There are several different avenues of regression that can be explored, ranging from hypothesis testing to model adequacy. Each of these methods involves the properties of the least squares estimators, which is the same procedure CART employs in a regression analysis. Since the target variable in this research is categorical, the classification analysis is used. However, regression analysis is used to validate the accuracy of the NOGAPS model (see Chapter 4).

3.4.2 *Simple Linear Regression.* The method of least squares approximates a line connecting points  $(X_1, Y_1), (X_2, Y_2) \dots (X_n, Y_n)$  which has the equation

$$\hat{Y} = \beta_0 + \beta_1 x_i + \varepsilon_i \quad (10)$$

where  $\hat{Y}$  is an approximation of the true  $Y$ ,  $\beta_0, \beta_1$  are coefficients of regression, and  $\varepsilon_i$  is a margin of error. The intercept,  $\beta_0$ , and slope,  $\beta_1$ , are defined as

$$\hat{\beta}_0 = \bar{y} - \hat{\beta}_1 \bar{x} \quad (11)$$

$$\hat{\beta}_1 = \frac{\sum_{i=1}^n y_i x_i - \frac{\left(\sum_{i=1}^n y_i\right)\left(\sum_{i=1}^n x_i\right)}{n}}{\sum_{i=1}^n x_i^2 - \frac{\left(\sum_{i=1}^n x_i\right)^2}{n}} \quad (12)$$

where  $\bar{y} = \frac{1}{n} \sum_{i=1}^n y_i$  and  $\bar{x} = \frac{1}{n} \sum_{i=1}^n x_i$  (Montgomery and Runger 2002). These equations

can therefore be extended to include  $j$  predictors in the domain of  $X$  (for multiple linear regression analyses). A scatter plot of data which yields a strong correlation between  $Y$  and  $X_i$  would have minimal errors,  $e_i$ , or residuals defined as

$$e_i = y_i - \hat{y}_i \quad (13)$$

since this is the difference between the estimated (regression) value of  $y$  and the true value of  $y$ . Using regression analysis requires the following assumptions discussed by Montgomery and Runger (2002). These assumptions allow the user to make inferences based on the regression, and the overall model capability is often noted by the  $R^2$  coefficient.

- 1) Estimation of the model parameters requires assumption that errors are uncorrelated random variables with mean zero and constant variance.
- 2) Tests of hypothesis and interval estimation require the errors be normally distributed.
- 3) The order of the model is correct, which assumes the phenomenon actually behaves in a linear or first-order manner.

The adequacy of the model can also be judged by the coefficient of determination  $R^2$ . Since there is no perfect model,  $R^2$  values rarely reach unity and higher values indicate better effectiveness. “Qualitatively, the  $R^2$  can be interpreted as the proportion of the variation of the predictand (proportional to  $SS_T$ ) that is “described” or “accounted for” by the regression ( $SS_R$ )” (Wilks 1995). In multiple linear regression, adding more predictors inherently increases  $R^2$ , and it can be difficult to determine whether the increase is providing useful information about the new predictor. Therefore  $R^2_{adj}$  is used to compensate for the number of parameters in a regression model. The equations for  $R^2$  and  $R^2_{adj}$  are shown in Equations 14 and 15

$$R^2 = \frac{SS_R}{SS_T} = 1 - \frac{SS_E}{SS_T} \quad (14)$$

$$R^2_{adj} = 1 - \frac{\frac{SS_E}{(n-p)}}{\frac{SS_T}{(n-1)}} \quad (15)$$

where  $SS_R$  is the regression sum of squares,  $SS_T$  is the total sum of squares,  $SS_E$  is the error sum of squares, and  $(n-p)$  and  $(n-1)$  are degrees of freedom (Montgomery and Runger 2002).

Another common measure of accuracy that can be used is the mean-squared error (MSE). The MSE averages the individual squared differences between the gridded forecast and observed fields at each of the  $M$  grid points. This is defined mathematically in Equation 16.

$$MSE = \frac{1}{M} \sum_{m=1}^M (y_m - o_m)^2 \quad (16)$$

“Often the MSE is expressed as its square root, the root-mean squared error (RMSE).

$$RMSE = \sqrt{MSE} \quad (17)$$

This form of expression has the advantage that it retains the units of the forecast variable and is thus more easily interpretable as a typical error magnitude” (Wilks 1995).



## **IV. Analysis and Results**

### *4.1 Introduction*

This chapter discusses the performance of the selected predictors from Chapter 3 and the results of the CART classification analyses. Initially, a simple linear regression study is done on the NOGAPS wind analyses to determine accuracy when compared to the BT data (i.e., nearest ground truth). This regression study determines how well the model depicts the changes in the environment that lead to rapid changes in typhoon intensity. In addition, a comparison could be done with MSLP and NOGAPS pressure analyses, however since pressure is not available in the BT data archive for the majority of this research, this study is not performed. The BT data archive starting with 2001 can be used in an MSLP regression assessment.

### *4.2 Regression Analysis of NOGAPS and Best Track Data*

It is important to establish confidence in the NOGAPS model early in the research, since it is the primary source of data. In general, model data are never used in determining BT data. NOGAPS is only used in cases where the standard techniques of determining maximum wind speed (Dvorak CI relationship, synoptic or microwave patterns) are not well fit to the storm, such as when typhoons are not well developed or as in a midget typhoon (Vilpors personal correspondence 2003). A description of midget typhoons can be found in the TC Forecasters' Reference Guide, NRL Website (1998).

The NOGAPS model employs a multivariate optimum interpolation analysis to include, but not limited to, radiosonde, aircraft, and satellite measurements. In addition, it should be noted that the analyses of TC are almost too large in horizontal extent due to the global model resolution (UCAR website 2004). Furthermore, since 1990, the data have been “bogused” to account for the position and intensity of a typhoon. Goerss and Jeffries (1994) provide further information as to the nature of bogusing the model.

In order to perform the initial regression analysis, the SAS Institute statistical software package JMP is used to determine RMSE and correlation strength between the NOGAPS wind analyses and the BT data. Table 9, sorted by typhoon name, shows a breakdown of these statistics, where a fit line technique is used in calculating RMSE. The RMSE values can also be calculated in a similar fashion by using a fit model analysis with standard least squares.

This initial analysis shows a fairly high correlation strength, however the regression fit line between NOGAPS and BT accounts for only 1/3 of the variance of the model. In fact, scatter plots of the BT data against time show more of an exponential rise whereas the NOGAPS data indicate a multi-ordered polynomial fit. It is probable that if a cubic, quadratic, or higher ordered fit is attempted, the RMSE values would decrease (i.e., for a better linear fit, there should be less variability in the data points). On average, the RMSE values indicate 24.849 kts variation between NOGAPS and BT data. Although the model handles the trends in the wind speeds well, there is an error of about 25 kts. However, given that a linear fit (and not higher ordered fit) is used, the NOGAPS model can be employed with a reasonable level of confidence that it is accurately depicting the typhoon surface wind strength.

Table 9. Initial regression analysis of NOGAPS and BT.

Typhoon Name	RMSE	Correlation Strength
02C97	28.455	0.7119
05C97	28.068	0.748
07W97	20.899	0.8652
10W97	25.468	0.774
17W97	17.072	0.5047
18W97	23.058	0.6562
24W97	25.239	0.7864
27W97	30.701	0.7078
28W97	32.899	0.7232
29W97	32.134	0.7316
05W99	25.272	0.5375
06W99	29.566	0.4089
16W99	17.258	0.1415
24W99	24.077	0.8262
26W99	27.495	0.459
04W01	22.566	0.2569
06W01	13.602	0.7469
10W01	22.578	0.4347
11W01	22.99	0.5975
12W01	24.431	0.7407
16W01	33.22	0.2656
20W01	21.808	0.2225
23W01	19.483	0.5723
24W01	22.216	0.5606
26W01	31.871	0.6948
27W01	20.114	0.8077
33W01	28.389	0.7157

### 4.3 Classification Tree Analysis

*4.3.1 Best Method Determination.* In order to maximize CART's effectiveness, each of the six-hourly fixes are merged into a single data set. This set contains 1198 records from which a variety of splits could be tested. It is also possible to vary the set of predictors used within each split. Since the Gini and Twoing methods are the most widely discussed in the literature, it is important to determine if these provide the best

results. However, a brief description of the other four available testing methods can be found in Salford Systems (2002). An initial screening of various predictor sets is run under Gini and Twoing, and the relative cost, percent error misclassification, and percent prediction success are documented in Tables 10 through 12.

Table 10. Initial screening of relative cost.

Predictor Set	Gini	Twoing
All predictors (no categorical, U, V)	<b>0.408</b>	0.436
All predictors (no categorical, SPD, DIR)	0.443	0.446
All predictors (with categorical no U, V)	0.431	0.448
All predictors (with categorical no SPD, DIR)	0.453	0.449

Table 11. Initial screening of percent error misclassification.

Predictor Set	Gini	Twoing
Class 0		
All predictors (no categorical, U, V)	31.53%	37.22%
All predictors (no categorical, SPD, DIR)	32.3%	34.52%
All predictors (with categorical no U, V)	32.69%	39.63%
All predictors (with categorical no SPD, DIR)	<b>24.49%</b>	37.61%
Class 1		
All predictors (no categorical, U, V)	27.03%	27.03%
All predictors (no categorical, SPD, DIR)	31.08%	27.03%
All predictors (with categorical no U, V)	27.03%	27.03%
All predictors (with categorical no SPD, DIR)	35.14%	<b>25.68%</b>
Class 2		
All predictors (no categorical, U, V)	<b>22.99%</b>	<b>22.99%</b>
All predictors (no categorical, SPD, DIR)	25.29%	27.59%
All predictors (with categorical no U, V)	26.44%	<b>22.99%</b>
All predictors (with categorical no SPD, DIR)	31.03%	26.44%

Table 12. Initial screening of percent prediction success.

Predictor Set	Gini	Twoing
Class 0		
All predictors (no categorical, U, V)	68.47%	62.78%
All predictors (no categorical, SPD, DIR)	67.7%	65.48%
All predictors (with categorical no U, V)	67.31%	60.37%
All predictors (with categorical no SPD, DIR)	<b>75.51%</b>	62.39%
Class 1		
All predictors (no categorical, U, V)	72.97%	72.97%
All predictors (no categorical, SPD, DIR)	68.92%	72.97%
All predictors (with categorical no U, V)	72.97%	72.97%
All predictors (with categorical no SPD, DIR)	64.86%	<b>74.32%</b>
Class 2		
All predictors (no categorical, U, V)	<b>77.01%</b>	<b>77.01%</b>
All predictors (no categorical, SPD, DIR)	74.71%	72.41%
All predictors (with categorical no U, V)	73.56%	<b>77.01%</b>
All predictors (with categorical no SPD, DIR)	68.97%	73.56%

The relative cost of the classification model is loosely interpreted as  $1 - R^2$ , in statistical terms, or the percent of error left unexplained by the tree as compared against the trivial model (where everything is classified under the largest class). In order to compute relative cost (RC), Equations 18 through 20 are used

$$E = \frac{1}{classes} \left( \frac{misclass\_0}{total\_0} + \frac{misclass\_1}{total\_1} + \frac{misclass\_2}{total\_2} \right) \quad (18)$$

$$E_{trivial} = \frac{1}{classes} (classes - 1) \quad (19)$$

$$RC = \frac{E}{E_{trivial}} \quad (20)$$

where  $misclass\_n$  is the number of misclassified records per Class  $n$ , and  $total\_n$  is the total of records per Class  $n$ . The overall goal is build a model where RC is very small or close to zero. Equation 20 is minimized when there is a large number of classes, and the

number of misclassified records per class is small. Percent error misclassification is the percent of the total records per Class  $n$  which are misclassified, and the percent prediction success is one minus the percent error misclassification. Bolded values in Tables 11 and 12 are considered the best per class and method. Since each level of SPD and DIR is computed from the U and V data at the same level, the overall predictor list is analyzed with a SPD and DIR subset as well as a U and V subset. This separation is done to evaluate any significance between using one version over the other; a single analysis would use the wind-based predictors twice instead of once. In addition, categorical (CAT) refers to unfavorable and favorable conditions of STSS and STDS.

The lowest percent error misclassification is 24.49% for Class 0, 25.68% for Class 1, and 22.99% for Class 2. The highest prediction success is 75.51% for Class 0, 74.32% for Class 1, and 77.01% for Class 2. In this analysis, there is a split between the Gini and Twoing methods as well as in the overall predictor set. Class 0 events have better results with the Gini method while Class 1 events have better results with the Twoing method. In addition, Class 2 events are split between the Gini and Twoing methods, and the lowest relative cost occurs with the Gini method. Furthermore, the different predictor sets are almost split evenly among the methods. This information is illustrated in Table 13 where the counts are determined from the bolded values in Tables 10 through 12.

It appears initially that there is no way to impartially choose between the sets without sacrificing some measure of accuracy in one or more classes. Therefore the changes in percent error misclassification between the sets and methods are examined. If there is minimal loss between switching to the values in one set and method over another,

then an overall “best” set and method can be used. In order to choose the lowest misclassification across the classes, the average of each predictor set and method are computed and shown in Table 14.

Table 13. Total counts of initial screening.

Predictor Set	Gini	Twoing
All predictors (no categorical, U, V)	3	2
All predictors (no categorical, SPD, DIR)	0	0
All predictors (with categorical no U, V)	0	2
All predictors (with categorical no SPD, DIR)	2	2

Table 14. Average percent error misclassification.

Predictor Set	Gini	Twoing
All predictors (no categorical, U, V)	<b>27.18%</b>	29.08%
All predictors (no categorical, SPD, DIR)	29.56%	29.71%
All predictors (with categorical no U, V)	28.72%	29.88%
All predictors (with categorical no SPD, DIR)	30.22%	29.91%

Not surprisingly, the ranking of these results match the ranking of the relative cost values in Table 10. Thus, the “best” predictor set is established as All predictors (no categorical, U, V) and the “best” method is Gini. Under this determination, Class 0 events gain 7.04% error misclassification, and Class 1 events gain 1.35% error misclassification. However, the percent error misclassification for Class 2 events remains the same. It is important to note that these analyses are run under the assumption that the distribution of classes in the population is equal (hence Priors Equal). This assumption provides the most unbiased handling of the data where every record has an equal chance of being classified in each of the target classes (Steinberg and Colla 1995 discuss each of the Priors methods available for testing). On the other hand, the

distribution of target classes from this population is known. Class 0 events comprise 1037 of 1198 records (~86.56%), Class 1 events comprise 74 of 1198 records (~6.18%), and Class 2 events comprise 87 of 1198 records (~7.26%). As a result, Class 0 events are approximately 13 times more prevalent than either Classes 1 or 2. With this understanding, a secondary analysis is run where the actual distribution of classes is taken into account.

After adjusting the analysis to reflect the estimated distribution frequency in each of the classes (i.e., setting the analysis to Priors Data), the percent error misclassification for Class 0 drops to 2.03%, and the percent error misclassification for Classes 1 and 2 rises to 68.92% and 78.16%, respectively. This analysis clearly shows that adjusting the priors in one class can dramatically affect the outcome in another class. Steinberg and Colla (1995) and Salford Systems (2002) suggest initially building trees under the default of Priors Equal such that the classes are treated as if they were uniformly distributed in the population regardless of their distribution in the sample. With an uneven distribution of classes in this research, using Priors Equal induces a cost structure that favors a rarer class in the data (hence Classes 1 and 2). Since it is important to provide an unbiased assessment of the predictors in any sample (i.e., data from other years), customizing the analysis to maximize the performance in one class is avoided, and Priors Equal is regarded as the correct way to treat the sample.

Another way to assess predictive power without tailoring the analysis is to change the target variable to a different predictor and compare those results against the TGT predictor. Three other predictors (CAT STSS, CAT STDS, and CH OUT) are selected as the target variable to see if improved percent error misclassification can be achieved.



Inferences towards the conditions needed for the ideal atmospheric state might be made if these results are better than the initial analysis with the TGT predictor. Tables 15 through 17 show the percent error misclassification for CAT STSS, CAT STDS, and CH OUT.

This secondary analysis, for categorical speed and directional shear, shows much improvement in percent error misclassification, and the analysis for channel outflows shows only slight improvement in percent prediction success. Given the higher accuracy in predicting categorical shear as the target variable, this examination is explored further.

Table 15. Percent error misclassification for CAT STSS.

Predictor Set	Gini	Twoing
Unfavorable		
All predictors (no CAT STDS, U, V)	3.72%	3.59%
All predictors (no CAT STDS, SPD, DIR)	3.47%	3.35%
All predictors (with CAT STDS no U, V)	3.35%	3.35%
All predictors (with CAT STDS no SPD, DIR)	3.35%	<b>3.22%</b>
Favorable		
All predictors (no CAT STDS, U, V)	8.95%	8.95%
All predictors (no CAT STDS, SPD, DIR)	7.16%	7.16%
All predictors (with CAT STDS no U, V)	<b>5.37%</b>	<b>5.37%</b>
All predictors (with CAT STDS no SPD, DIR)	6.91%	6.91%

Table 16. Percent error misclassification for CAT STDS.

Predictor Set	Gini	Twoing
Unfavorable		
All predictors (no CAT STSS, U, V)	<b>1.89%</b>	<b>1.89%</b>
All predictors (no CAT STSS, SPD, DIR)	2.16%	2.16%
All predictors (with CAT STSS no U, V)	1.35%	1.35%
All predictors (with CAT STSS no SPD, DIR)	1.35%	1.35%
Favorable		
All predictors (no CAT STSS, U, V)	4.82%	4.82%
All predictors (no CAT STSS, SPD, DIR)	4.82%	4.82%
All predictors (with CAT STSS no U, V)	<b>2.19%</b>	<b>2.19%</b>
All predictors (with CAT STSS no SPD, DIR)	<b>2.19%</b>	<b>2.19%</b>

Table 17. Percent error misclassification for CH OUT.

Predictor Set	Gini	Twoing
No Outflow		
All predictors (no categorical, U, V)	21.81%	20.66%
All predictors (no categorical, SPD, DIR)	19.01%	<b>17.35%</b>
All predictors (with categorical no U, V)	21.81%	20.66%
All predictors (with categorical no SPD, DIR)	19.13%	20.92%
Single		
All predictors (no categorical, U, V)	20%	18.31%
All predictors (no categorical, SPD, DIR)	21.97%	18.31%
All predictors (with categorical no U, V)	20%	18.31%
All predictors (with categorical no SPD, DIR)	21.41%	<b>16.61%</b>
Double		
All predictors (no categorical, U, V)	26.09%	26.09%
All predictors (no categorical, SPD, DIR)	<b>21.74%</b>	23.91%
All predictors (with categorical no U, V)	26.09%	26.09%
All predictors (with categorical no SPD, DIR)	<b>21.74%</b>	<b>21.74%</b>

*4.3.2 Alternate Target Classification Tree Results.* The alternate targets (CAT STSS and CAT STDS) show interesting, but not highly useful results from which inferences towards the primary target can be made. Figures 15 and 16 show the classification tree for each target. In each figure, a color coding scheme is employed where green indicates an internal node, red indicates higher purity in a terminal node, blue indicates lower purity in a terminal node, and colors between red and blue depict gradients in the purity levels of terminal nodes. Both figures are displayed with the color code oriented towards favorable shear. Each figure also contains a number corresponding to each terminal node in the tree. In addition, Tables 18 and 19 show a breakdown of terminal node details for each tree.

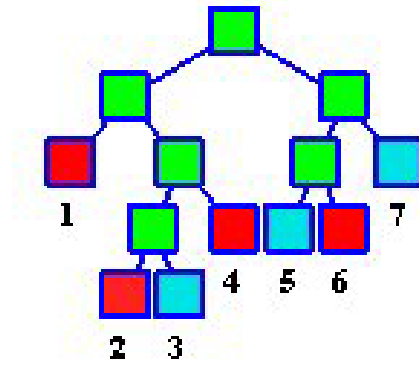


Figure 15. Classification tree for CAT STSS.

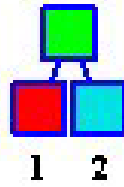


Figure 16. Classification tree for CAT STDS.

Table 18. Terminal node details for CAT STSS.

Terminal Node	Node Purity per Class		Number of Records per Class	
	U	F	U	F
1	3%	97%	11	<b>351</b>
2	33.3%	66.7%	1	2
3	100%	0%	15	0
4	16.7%	83.3%	3	<b>15</b>
5	93.8%	6.2%	76	5
6	8.3%	91.7%	1	<b>11</b>
7	99%	1%	700	7

Table 19. Terminal node details for CAT STDS.

Terminal Node	Node Purity per Class		Number of Records per Class	
	U	F	U	F
1	1.8%	98.2%	8	<b>446</b>
2	98.7%	1.3%	734	10

The highest purity terminal nodes for CAT STSS are Node 1 with 351 records, Node 4 with 15 records, and Node 6 with 11 records. An examination of the splitting rules for each node is portrayed in Table 20. The highest purity terminal node for CAT STDS is Node 1 with 446 records; the splitting rules for this node are found in Table 21.

Table 20. Splitting rules for CAT STSS.

Terminal Node	Splitting Rules
1	$TTSS \leq 15.825$
4	CAT STDS is favorable && $TTSS > 15.825$ && $TTSS \leq 16.16$
6	$TTSS > 16.61$ && $TTSS \leq 18.79$ && $E50 SPD > 31.92$

Table 21. Splitting rules for CAT STDS.

Terminal Node	Splitting Rules
1	$TTDS \leq 44.965$

Although the purity levels are high for each target variable, the amount of information gleaned from the splitting rules is minimal. Only one terminal node in each target contains a substantial quantity of records despite other nodes (within CAT STSS) having purity levels in excess of 80%. However, this limitation should not be discarded all together. The analysis confirms JTWC's guidance on speed and directional shear (i.e., 15 kts and 45 deg for favorable conditions), and the levels needed to compute shear can now be extended to 1000-200 mb versus only examining surface-200 mb. These results are helpful if there is high confidence in predicting rapid intensification and

weakening based on TTSS and TTDS. Otherwise, inferring changes based on the alternate target variables (CAT STSS, CAT STDS, and CH OUT) do not provide significant impact to the forecast process. The results based on the primary target are illustrated in greater depth in the next section.

*4.3.3 Primary Target Classification Tree Results.* An initial examination of the primary target results yields a wide variety of terminal nodes. Figures 17 through 19 show the color coding scheme based on Classes 2, 1, and 0. This color scheme is exactly the same as discussed in the previous section. These figures illustrate that the highest concentration of purity in the tree is focused towards Class 0 events. Class 1 and 2 events comprise a much smaller concentration of purity within the overall structure. Terminal node details for the TGT tree are found in Table 22.

Another useful examination of the TGT tree can be found in the variable importance table. This table shows the hierarchy of predictor importance with respect to improvement scores. During the tree building process, each predictor is examined as the primary splitter, and the improvement score associated with that split is kept in memory. Once the optimal tree is grown, the improvement scores are summed over all predictors, the most important predictor receiving a score of 100. Every predictor listed below the top variable has a score which is considered a certain fraction of importance to the overall tree building process. The variable importance table for the TGT tree is portrayed in Table 23.

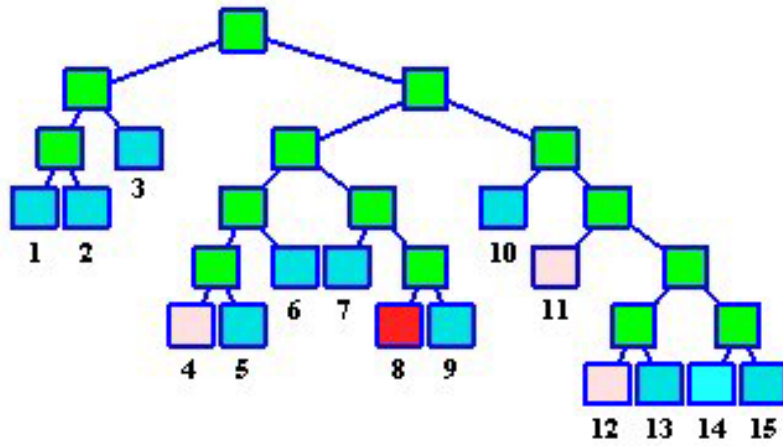


Figure 17. Classification tree for TGT (Class 2).

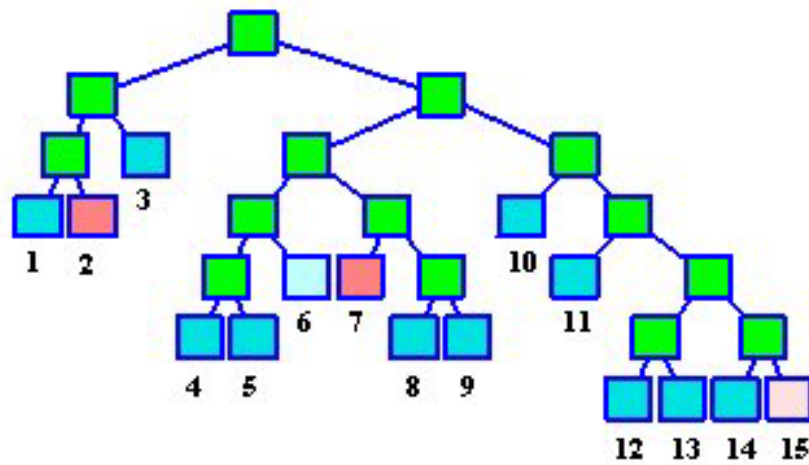


Figure 18. Classification tree for TGT (Class 1).

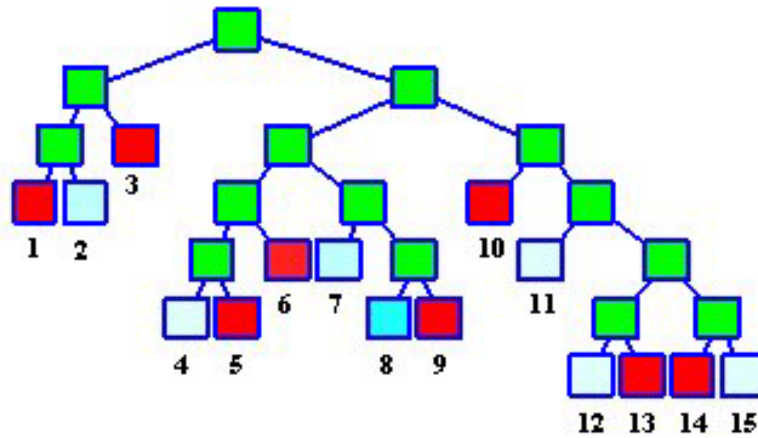


Figure 19. Classification tree for TGT (Class 0).

Table 22. Terminal node details for TGT.

Terminal Node	Node Purity per Class			Number of Records per Class		
	0	1	2	0	1	2
1	98.4%	0%	1.6%	60	0	1
2	61.9%	36.6%	1.5%	83	49	2
3	99%	1%	0%	98	1	0
4	70.4%	1.5%	28.1%	143	3	57
5	100%	0%	0%	22	0	0
6	96.4%	3.6%	0%	27	1	0
7	64.3%	35.7%	0%	9	5	0
8	42.9%	0%	57.1%	3	0	4
9	97.5%	1.3%	1.2%	78	1	1
10	100%	0%	0%	270	0	0
11	80.6%	0%	19.4%	54	0	13
12	75%	0%	25%	24	0	8
13	100%	0%	0%	60	0	0
14	98%	0%	2%	50	0	1
15	80%	20%	0%	56	14	0

The predictors which have a score of zero do not have any impact, and predictors with scores close to zero contribute little to the tree architecture. In order to improve the relative cost of this analysis, the lower importance variables are systematically removed,

and a new tree is grown. It is important to note that removing too many predictors can actually result in a higher relative cost. Thus, there is an optimal set of predictors which should be used to minimize the relative cost and overall misclassification rate. After analyzing multiple predictor sets, the variables associated with the lowest overall relative cost are displayed in Table 24.

This particular set of predictors yields a relative cost of 0.322 with a misclassification rate of 29.12% for Class 0, 13.51% for Class 1, and 21.84% for Class 2. When these results are compared to the initial screening results, the absolute change in misclassification rate is +4.63% for Class 0, -12.17% for Class 1, and -1.15% for Class 2. Therefore, it is clear that a substantial gain in predictability is achieved for rapidly weakening events, and a slight gain in predictability is achieved for rapidly intensifying events. However, the improvement in both of these classes comes at a slight increase in the misclassification of events where no rapid change is occurring. Since the majority of focus should be placed upon an environment conducive to rapid change versus a more stagnant or slowly changing environment, these results are insightful. If misclassification is thought of in terms of false alarm rate, using the refined list of predictors (or list of critical predictors) should yield 70.88% accuracy in predicting typhoon rapid intensification and 86.49% accuracy in predicting typhoon rapid weakening. In order to visualize these results, Figures 20 through 22 show the new classification trees per focus class, and Figure 23 shows the splitter at each internal node.



Table 23. Variable importance for TGT.

Variable Name	Score
LAT	100.00
SFC T	84.87
E50 T	66.52
E50 RH	55.79
SST	53.28
AGE	52.44
THSN T	47.96
TWO T	33.83
SOI	25.54
MEI	23.33
CH OUT	21.23
STSS	19.59
CLIMO	16.07
TTSS	14.84
SFC SPD	14.59
TWO DIR	13.3
THSN RH	10.25
ETSS	9.22
THSN SPD	8.61
TWO SPD	7.1
TTDS	4.76
E50 DIR	2.16
STDS	0.65
E50 SPD	0.00
SFC DIR	0.00
THSN DIR	0.00
ETDS	0.00
MONTH	0.00
SFC RH	0.00
TUTT	0.00
O HEMI	0.00

Table 24. Refined variable importance for TGT.

Variable Name	Score
LAT	100.00
AGE	64.25
SFC T	60.44
SST	59.08
E50 T	46.01
TWO T	44.9
MEI	35.23

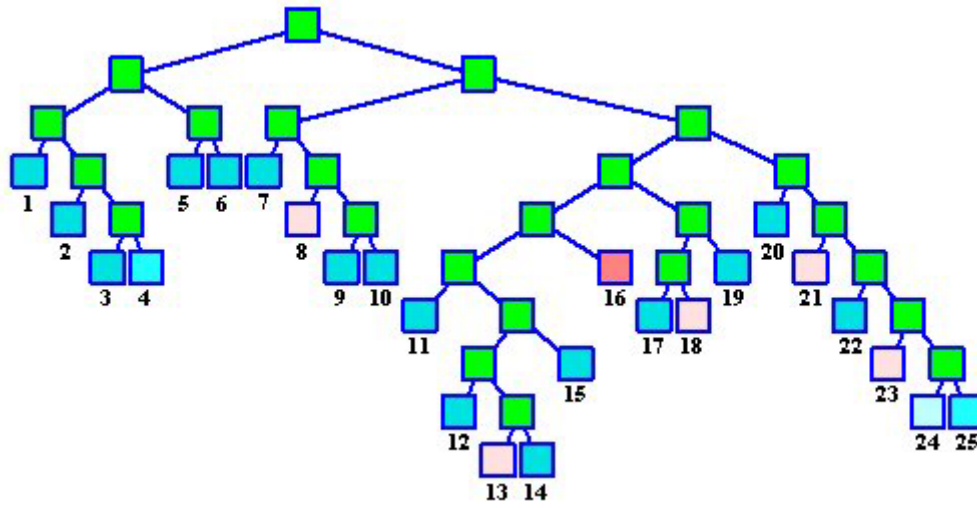


Figure 20. New classification tree for TGT (Class 2).

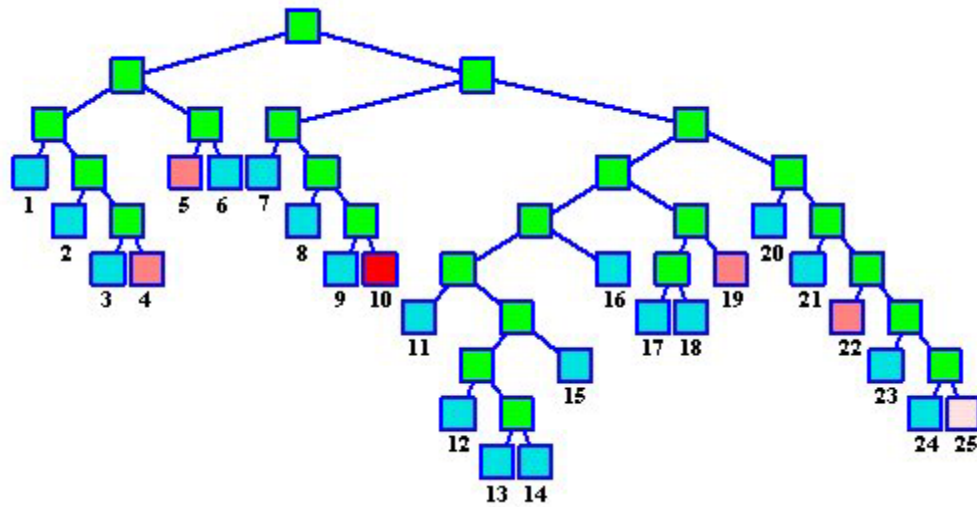


Figure 21. New classification tree for TGT (Class 1).

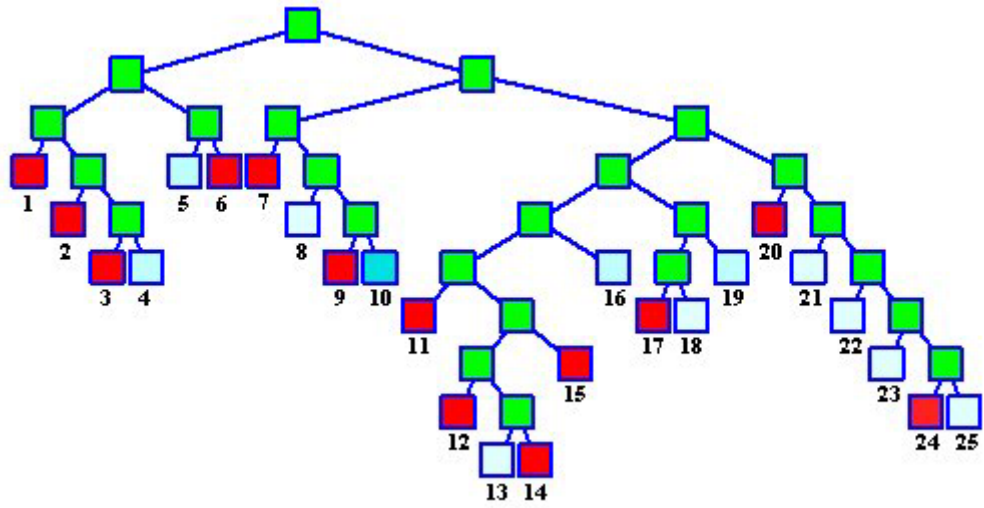


Figure 22. New classification tree for TGT (Class 0).

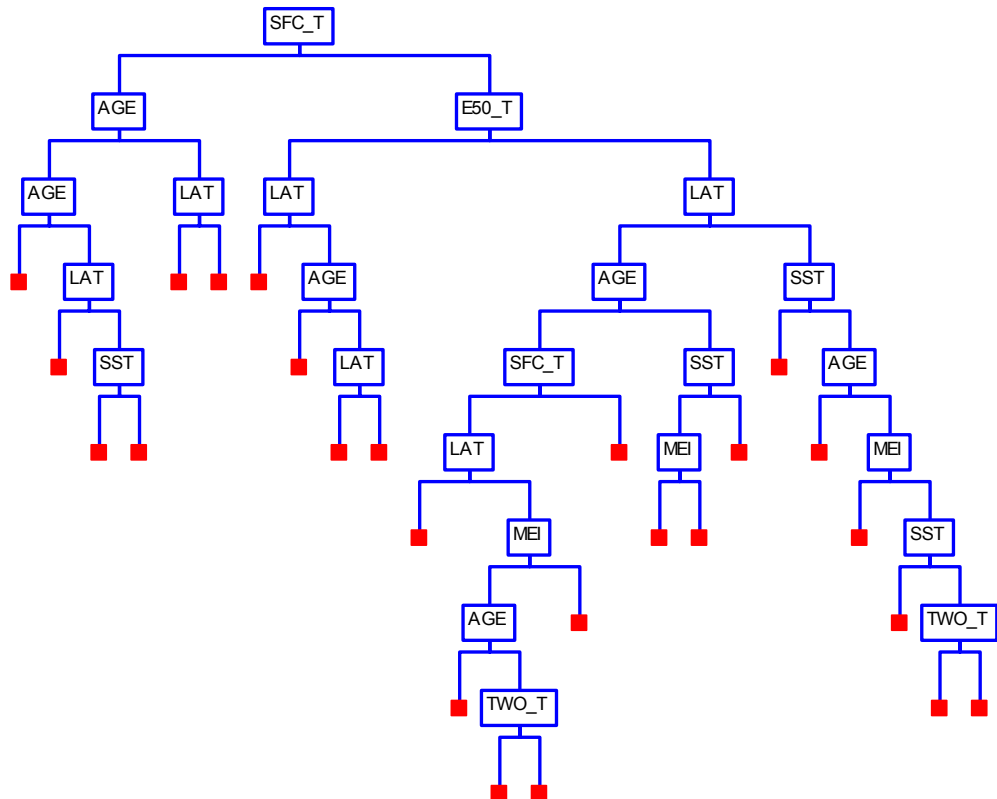


Figure 23. Splitters for new classification tree.

Similar to Figures 17 through 19, the highest concentration of purity in the tree is focused towards Class 0 events. Class 1 and 2 events comprise a much smaller amount of homogeneity within the overall structure. The new terminal node details are found in Table 25. This table shows a relatively even distribution of Class 0 records in each of the terminal nodes, except for Node 7 which has 206 records. Class 1 records are located mainly in Node 4 while the largest quantity of Class 2 records are dispersed between Nodes 13, 16, and 19. Since the primary focus is towards predicting Class 1 and 2 events, and these events are not situated in the same terminal nodes, an examination of the splitting rules is accomplished. Table 26 shows the splitting rules for each of the nodes which have the greatest number of records in Class 1 and 2. This examination is done to determine the highest occurrence of the same rule or type of rule. For example, if a criteria is split on a certain value, it is essential to draw this information out and examine it based on meteorological soundness.

The summation of records in Table 26 is 71 for Class 1 and 73 for Class 2. This number represents 95.95% and 83.91% of the total number available in each class, respectively. Table 26 also denotes the largest groups of records in each class from Table 25 (bolded values). The remaining records in Table 25 are few and dispersed among the rest of the terminal nodes. In order to develop a concise forecast decision tree, the nodes with only a couple of records are not reflected in Table 26. However, the splitting rules for the entire tree (i.e., across all terminal nodes) can be found in Appendix C.

Given the variety of splitting rules in Table 26, it is crucial to evaluate each one based on meteorological soundness. For example, the splitting rules for SFC T in Class 1 events (rapid weakening) show  $SFC\ T \geq 26.89$  and  $SFC\ T < 26.89$ . Only one of these

conditions supports a logical forecast decision while the other condition does not. In this situation, surface temperatures which are colder would be favorable for rapid weakening. In order to fairly decide which rules should be discarded, the distribution of each predictor is examined. The distribution shows the mean of each predictor by class as well as other statistical information (i.e., histogram, box and whiskers plot, outliers). Distributions for each class are shown in Figures 24 and 25, and Table 27 displays the moments information taken from the analyze distribution module in JMP.

Table 25. New terminal node details for TGT.

Terminal Node	Node Purity per Class			Number of Records per Class		
	0	1	2	0	1	2
1	98.4%	0%	1.6%	60	0	1
2	100%	0%	0%	13	0	0
3	100%	0%	0%	13	0	0
4	52.8%	45.4%	1.9%	57	<b>49</b>	2
5	50%	50%	0%	1	1	0
6	100%	0%	0%	97	0	0
7	100%	0%	0%	206	0	0
8	80%	0%	20%	20	0	<b>5</b>
9	100%	0%	0%	27	0	0
10	0%	100%	0%	0	1	0
11	98.7%	0%	1.3%	74	0	1
12	100%	0%	0%	16	0	0
13	73%	1%	26%	76	1	<b>27</b>
14	100%	0%	0%	16	0	0
15	100%	0%	0%	41	0	0
16	58.6%	0%	41.4%	51	0	<b>36</b>
17	100%	0%	0%	92	0	0
18	78.3%	0%	21.7%	18	0	<b>5</b>
19	60%	40%	0%	9	<b>6</b>	0
20	100%	0%	0%	54	0	0
21	77.8%	0%	22.8%	14	0	4
22	69%	31%	0%	20	<b>9</b>	0
23	83.3%	0%	16.7%	20	0	4
24	95.2%	0%	4.8%	20	0	1
25	73.3%	23.3%	3.4%	22	<b>7</b>	1

Table 26. Class 1 and Class 2 splitting rules.

# Records	Class 1 Splitting Rules	# Records	Class 2 Splitting Rules
49 (Node 4)	SFC T $\leq$ 26.89 & AGE > 13.5 & AGE $\leq$ 45.5 & LAT > 13 & SST > 18.5	36 (Node 16)	E50 T > 18.99 & LAT $\leq$ 21.35 & AGE $\leq$ 36.5 & SFC T > 31.89
9 (Node 22)	SFC T > 26.89 & E50 T > 18.99 & LAT > 21.35 & SST > 23.5 & AGE > 14.5 & MEI $\leq$ -0.239	27 (Node 13)	E50 T > 18.99 & SFC T > 26.89 & SFC T $\leq$ 31.89 & LAT > 13.15 & LAT $\leq$ 21.35 & MEI $\leq$ 2.589 & AGE > 5.5 & AGE $\leq$ 36.5 & TWO T $\leq$ -47.81
7 (Node 25)	SFC T > 26.89 & E50 T > 18.99 & LAT > 21.35 & AGE > 14.5 & MEI > -0.239 & SST > 26.45 & TWO T > -49.31	5 (Node 8)	SFC T > 26.89 & E50 T $\leq$ 18.99 & LAT > 17.7 & AGE $\leq$ 17
6 (Node 19)	SFC T > 26.89 & E50 T > 18.99 & LAT $\leq$ 21.35 & AGE > 36.5 & SST > 28	5 (Node 18)	SFC T > 26.89 & E50 T > 18.99 & LAT $\leq$ 21.35 & AGE > 36.5 & SST $\leq$ 28 & MEI > 2.6325

Table 27. JMP moments table for class distributions.

Class 1 Mean						
AGE	LAT	SFC T	E50 T	TWO T	SST	MEI
31.45	24.27	25.89	19.12	-49.33	25.73	0.292
Class 2 Mean						
AGE	LAT	SFC T	E50 T	TWO T	SST	MEI
22.13	17.52	32.13	22.33	-50.33	27.58	0.914

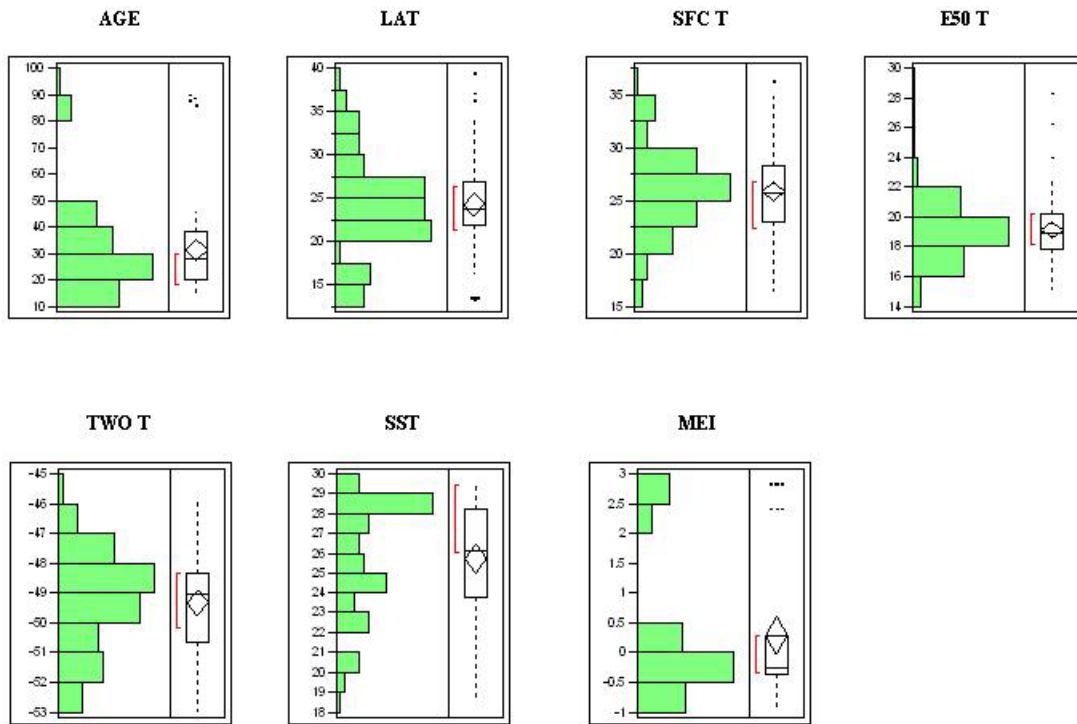


Figure 24. JMP distribution of Class 1.

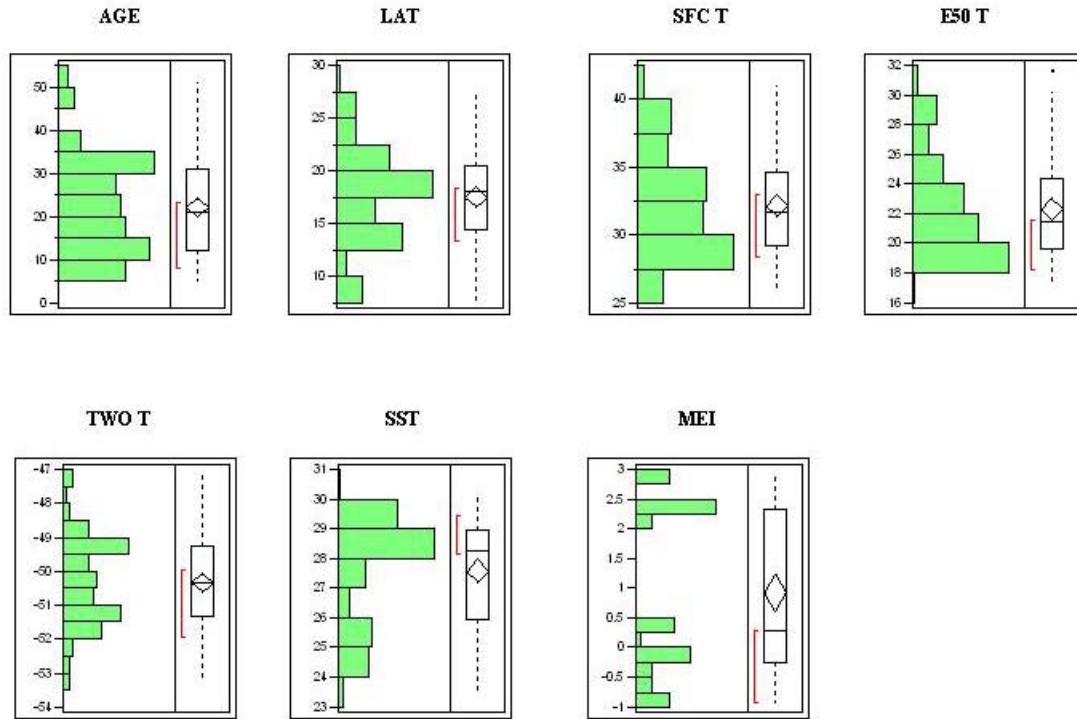


Figure 25. JMP distribution of Class 2.

The mean of each predictor is used as a threshold for determining the meteorological soundness of the CART splitting rule. Since there are instances of conflicting conditions, the mean provides the basis to further refine the splitting rule. Additionally, if the splitting rule is not consistent with the predictor mean, it should be discarded. For example, the splitting rule might suggest a criteria which would not be expected meteorologically (e.g., cold temperatures for rapid intensification). However, if the splitting rule makes logical sense, it should be kept.

The criteria established in Table 28 are the average of the means of the predictor in each class according to distributions in Table 27. The mean is used such that if the splitting rule meets these criteria (i.e., the mean brings the splitting rule “into agreement”), then conditions are favorable for that class. If the splitting rule does not meet these criteria, then conditions are deemed unfavorable, and the rule should be discarded. The values do not incorporate the effects of Class 0 events because the objective is to determine the validity of a splitting rule for Class 1 and 2 events. The rationale for using the criteria in Table 28 is described as follows:

AGE:	Rapid intensification more favorable during earlier stage in lifecycle.
LAT:	Rapid intensification more favorable in lower latitudes.
SFC T:	Rapid intensification more favorable with warmer temperatures.
E50 T:	Rapid intensification more favorable with warmer temperatures.
TWO T:	Rapid intensification more favorable with warmer temperatures.
SST:	Rapid intensification more favorable with warmer temperatures.
MEI:	Rapid intensification more favorable with positive values.

A typhoon has more time to develop in the earlier stages of the lifecycle than it does in the later stage of the lifecycle. Also, typhoons which reside in lower latitudes are not



subject to mid-latitude westerlies and enhanced shear, thus should have higher probability of intensification. Moreover, higher temperatures at the surface, 850 mb, and 200 mb are needed for maximized latent heat release which promotes stronger Cb development in the eyewall. Warmer 200 mb temperatures are indicative of a warm core low at the surface which implies vertically stacking and less baroclinicity. Temperatures which are colder might not be as indicative of a warm core low and imply more baroclinicity, thus unfavorable for typhoon development. It is important to note that colder cloud tops would be favorable for overall typhoon growth due to increased vertical motion;

Table 28. Criteria used to determine validity of splitting rule.

	Class 1	Class 2
AGE	$\geq 26.79$	$< 26.79$
LAT	$\geq 20.9$	$< 20.9$
SFC T	$< 29.01$	$\geq 29.01$
E50 T	$< 20.73$	$\geq 20.73$
TWO T	$< -49.83$	$\geq -49.83$
SST	$< 26.66$	$\geq 26.66$
MEI	$< 0.603$	$\geq 0.603$

However, this notion shouldn't be applied to a constant pressure surface. Finally, it has been shown that typhoons which develop during EN years live longer and are usually more dynamic (in terms of conditions needed for rapid growth), thus MEI values which are more positive support EN climatic regimes.

An examination of Table 26 according to the criteria set forth in Table 28 shows that for Class 1 events, 21.74% of the rules are correct, 60.87% of the rules are partially correct, and 17.39% of the rules are incorrect. The results for Class 2 events indicate 13.04% of the rules are correct, 78.26% of the rules are partially correct, and 8.7% of the

rules are incorrect. The rules which are partially correct contain a range of values where the threshold does and does not apply. For example, in Terminal Node 4, the splitting rule for AGE is  $> 13.5$  &  $\leq 45.5$ . This rule is partially correct since the threshold criteria for AGE is  $\geq 26.79$ . Since the majority of the splitting rules are deemed only partially correct (in agreement with the predictor means), it is essential for the forecaster to use experience and sound judgment in determining applicability of the rule. The only guideline in determining correct or incorrect rules is the arithmetic mean of the class distribution. However, it is encouraging to see 82.61% of Class 1 and 91.3% of Class 2 events denoted as either correct or partially correct. These percentages show high confidence in determining intensification trends.

#### *4.4 Supplement to the Intensity Analysis Worksheet and Verification*

The intensity analysis worksheet, shown in Table 29, reflects parameters that JTWC uses along with model consensus forecasting. The criteria are dominant in Dvorak analysis as well as satellite interpretation. In addition, the worksheet incorporates changes in sea surface temperatures as well as interactions with outflow channels and TUTT cells. However, this intensity analysis does not include NOGAPS model output.

The inclusion of model data is most likely dictated by the consensus forecasting technique. Since the majority of the parameters in Table 29 are not utilized in the CART analysis, they are still considered important features to the TC forecast process. In addition to these parameters, the forecast guidance in Table 30 is suggested as a supplement. This forecast guidance incorporates the correct and partially correct splitting

rules and adjusts the partially correct rules to reflect the validity criteria in Table 28. For example, Node 22 splitting rules state  $SFC\ T > 26.89$ , however the validity criteria suggests  $SFC\ T < 29.01$ . Therefore, a “smoothed” rule is established as  $SFC\ T > 26.89$  and  $SFC\ T < 29.01$ . This particular adjustment is employed in order to bring each of the partially correct splitting rules into agreement with the validity criteria. Each of the nodes are compared, and a generalized set of forecasting rules is developed for each class. These rules are listed in Table 30, and the predictors are organized in order of importance as determined by CART.

In order to verify the accuracy and usefulness of the forecast splitting rules (FSR), the criteria at six hours prior to the onset of Class 1 and 2 events were compared to the FSR. Since the research approach did not specifically incorporate any forecast time, the closest possible time to the event was used. Furthermore, if the six hour timeframe before the event contained any missing information, an average of the current and the next previous timeframe was used. For example, if the event was at 1800 UTC, but 1200 UTC data were missing, an average of 1800 UTC and 0600 UTC were used.

The verification of the FSR is illustrated in Table 31, where 1 indicates the variable criteria are met, and 0 indicates the variable criteria are not met. Table 32 shows the accuracy of the FSR. The total number of typhoons with at least one Class 1 event is 18 of 27 and at least one Class 2 event is 19 of 27. In a situation where the same class occurs more than once during the lifecycle of the storm, the first instance of the class is used. In addition, it is important to note that TWO T is not validated for Class 1 events because the CART splitting rule for this predictor is deemed incorrect.

Table 29. TC intensity analysis worksheet (modified from JTWC Website, 2003).

Criteria	Total Points Possible
Dvorak CI 3.0 to 4.0	2
Dvorak CI 4.0 to 5.0	0
200 mb anticyclonic outflow indicated over LLCC	1
200 mb cyclone indicated over LLCC	2
No organized 200 mb outflow indicated over LLCC	-1
No outflow channels present	-2
Single poleward outflow channel present	1
Single equatorward outflow channel present	2
Anticyclones in both hemispheres and adjacent to the TC (Equatorward outflow channel must also be present)	3
Dual outflow channels present	4
TUTT cell located NW (within 10 to 12 degrees of center)	5
TC moving over warmer SSTs ( $> 26^{\circ}\text{C}$ )	1
TC Q/S for more than 18 hours (sea surface mixing)	-2
TC moving over cooler SSTs ( $< 24^{\circ}\text{C}$ )	-3
Dvorak trend is W1.5 to W1.0 in 24 hours	-4
Dvorak trend is W0.5 to S0.0 in 24 hours	-2
Dvorak trend is D0.5 to D1.0 in 24 hours	0
Dvorak trend is $\geq$ D1.5 in 24 hours	2
Central dense overcast (CDO) present	2
Central cold cover (CCC) present	-2
<b>ASSESSMENT</b>	
$\geq 8$ :	Rapid development - forecast 1.5 T-number or greater
4 to 7:	Climatic development - forecast 1.0 T-number
-5 to 3:	Slow/steady development - forecast 0.5 T-number or less
-6 to -17:	Weakening

Table 30. Suggested forecast splitting rules. Precision reduced for ease of use.

Priority Level	Variable Name	Class 1	Class 2
1	LAT	$> 21^{\circ}\text{N}$	$\leq 21^{\circ}\text{N}$
2	AGE	$> 27$	$\leq 27$
3	SFC T	$\leq 29^{\circ}\text{C}$	$> 29^{\circ}\text{C}$
4	SST	$\leq 27^{\circ}\text{C}$	$> 27^{\circ}\text{C}$
5	E50 T	$\leq 21^{\circ}\text{C}$	$> 21^{\circ}\text{C}$
6	TWO T	n/a	$\geq -50^{\circ}\text{C}$
7	MEI	$\leq 0.6$	$> 0.6$

Table 31. Verification counts of the forecast splitting rules.

Variable																			
Level	Name	Class 1																	
1	LAT	0	0	1	0	1	1	1	0	0	1	1	1	1	0	1	1	0	0
2	AGE	1	0	1	0	0	0	1	0	0	0	1	0	1	0	1	1	0	1
3	SFC T	0	1	0	1	1	0	1	1	0	1	0	0	0	0	1	1	0	0
4	SST	0	1	1	0	1	0	1	0	0	0	0	0	0	0	1	0	0	0
5	E50 T	0	1	0	0	1	1	1	1	1	1	0	0	1	1	1	1	1	0
6	TWO T	-	-	-	-	-	-	-	-	-	-	-	-	-	-	-	-	-	-
7	MEI	0	0	0	1	1	1	1	1	1	1	1	1	1	1	1	1	1	1

Variable																			
Level	Name	Class 2																	
1	LAT	1	1	1	1	1	1	1	1	0	1	1	1	1	1	0	1	1	1
2	AGE	0	0	1	1	1	1	0	1	1	1	1	1	1	1	1	1	1	0
3	SFC T	1	1	1	1	1	1	0	0	0	0	0	0	1	1	1	0	1	1
4	SST	0	1	0	1	0	1	0	1	1	1	1	1	1	1	1	1	1	1
5	E50 T	1	0	1	1	1	0	0	0	0	0	0	0	0	1	0	0	0	1
6	TWO T	0	0	1	1	0	0	0	0	0	0	1	1	0	0	1	1	0	0
7	MEI	1	1	1	1	1	1	1	0	0	0	0	0	0	0	0	0	0	0

Table 32. Accuracy of the forecast splitting rules.

Priority Level	Variable Name	Class 1	Class 2
1	LAT	55.56% (10/18)	89.47% (17/19)
2	AGE	44.44% (8/18)	78.95% (15/19)
3	SFC T	44.44% (8/18)	63.16% (12/19)
4	SST	27.78% (5/18)	78.95% (15/19)
5	E50 T	66.67% (12/18)	31.58% (6/19)
6	TWO T	n/a	31.58% (6/19)
7	MEI	83.33% (15/18)	36.84% (7/19)
Average Percentage		53.7% (58/108)	58.65% (78/133)

FSR verification indicates 53.7% accuracy in predicting conditions favorable for rapid weakening and 58.65% accuracy in predicting conditions favorable for rapid intensification. Despite the “poor” performance of the FSR as a whole, it is interesting to note that the combined accuracy of the top three predictors is 82.46% (47 of 57) for Class

2 events and 68.52% (37 of 54) for Class 1 events. The predictors in Class 2 comprise priority levels 1, 2, and 4 while the predictors in Class 1 comprise priority levels 7, 5, and 1. This comparison suggests the priority levels should be redefined based on FSR accuracy rather than the CART variable importance table. The predictors (in order of importance) which should be given the most weight are LAT, AGE, and SST for Class 2 and MEI, E50 T, and LAT for Class 1. The other predictors in each class shouldn't necessarily be disregarded, however the predictive power might not be as great.

The rules established in Table 30 are only suggestions based on a combination of CART analysis splitting rules and validity criteria. An analyst still needs to use discretion while taking the FSR and the intensity analysis worksheet into consideration. In addition, not all of the rules are required for each forecasting scenario since not every predictor was used in each of the nodes listed in Table 26. Sound forecast judgment should prevail when opting to utilize one, two, or all of these rules. Furthermore, these rules are based on an exact split criteria, and this particular value can be adjusted given the environmental conditions present. If only a proportion of the suggested FSR is used, more weight should be given to the higher accuracy variables.

These rules are verified at the closest timeframe to the event occurring (i.e., six hours before intensification and weakening). Given the potential variability in the model parameters at some time in the future, it is probable that not all of the criteria will be met at the same time or over the same location. These rules are formulated as suggestive criteria, and forecaster judgment must always take higher priority. However, despite the 70% to 80% levels of accuracy, the rules shed light as to which model parameters have more predictive power, and they provide an enhancement to the forecast process.

## **V. Conclusions and Recommendations**

### *5.1 Conclusions*

The overall goal of this research was to data mine atmospheric parameters responsible for typhoon rapid intensification and weakening and to validate the usefulness of using these parameters in the forecast process. The primary method used to meet this goal was classification tree analyses. This research used components of the NOGAPS model along with numerous other atmospheric and climatic predictors. In addition to this examination, several minor objectives listed in Section 1.2 were also achieved.

The first objective was to gather all types of satellite imagery (visible, water vapor, and infrared) since satellite interrogation has become one of the primary tools in analyzing Northwest Pacific typhoons. Due to the availability of data covering the areas of interest, only infrared imagery from the Australian BOM was used. The data from the NRL did not provide enough of a synoptic-scale view to glean the necessary information. The infrared imagery provided a means of determining channel outflow patterns and when used with archived model fields from NCEP, interactions with TUTT cells and opposite hemispheric effects were verified.

The second objective was to collect the BT data which were obtained from JTWC. These data were vital in establishing the specific times associated with rapid weakening and intensification events (Class 1 and 2 events). The BT data also provided the specific timelines from which to gather NOGAPS model fields (objective 3). Each of

the records in the database were time matched with specific model data as well as subjective calls in the form of binary responses (0 for “no” and 1 for “yes”).

Temperature, relative humidity, and wind components (U and V) were the primary fields used from the NOGAPS model. The U and V components established speed and directional shear at different levels.

Inclusion of climatological effects comprised the fourth objective of the research. The early hypothesis that EN and LN regimes might have some influence on intensification trends was verified in this work. Furthermore, relationships between TUTT cells and climatic regimes were established. Although none of the 1999 storms had any interactions with the TUTT, both the 1997 and 2001 seasons showed typhoons which interacted with tropical upper level troughs.

The final objective was to examine relationships between the various predictors by using CART analyses. Since the target variable was defined categorically, a classification analysis was utilized. However, simple linear regression was used to compare the NOGAPS analyses of surface wind speed to the BT surface wind speeds. The classification analyses revealed interesting relationships between the target variable and the predictors. Some of the predictors, which were initially thought to play a vital role (such as speed, directional shear, and channel outflows) were revealed as less important, and some of the predictors which were not initially considered important became key players in the architecture of the classification tree importance. Nonetheless, it was a synergy of seven predictors (AGE, LAT, SFC T, E50 T, TWO T, SST, and MEI) which shed new light into when and under what conditions typhoons seem to intensify.



Using classification analyses to determine tropical cyclone intensification trends is feasible. The results, while not excellent at present, are promising in the data mining process. The original tree contains a percent error misclassification of 24.49% for Class 0, 25.68% for Class 1, and 22.99% for Class 2 events. After refining the predictor list (by systematically removing weaker predictors, which increase the relative cost), the percent error misclassifications become 29.12% for Class 0, 13.51% for Class 1, and 21.84% for Class 2 events. These new percentages are slightly different than the percent accuracy found in the verification process.

The verification process used the FSR as a basis for determining Class 1 and Class 2 events. The FSR as a whole showed an accuracy of 53.7% for Class 1 and 58.65% in Class 2 events. Verification in Class 0 was not done because this class represented neither rapid intensification nor rapid weakening (i.e., not one of the classes of interest). In addition to the complete FSR accuracy, the top three predictors in each class yielded 68.52% accuracy for Class 1 and 82.46% accuracy for Class 2 events.

In essence, the percent error misclassification and the FSR verification represent two different measures of the classification tree feasibility. The misclassification rates demonstrate the ability of the tree to accurately filter each of the classes into terminal nodes with the proper class assignments. The verification process characterizes the accuracy of using each parameter in the FSR against the actual events. Since neither set of percentages (misclassification nor verification) show a dominating level of accuracy, the overall performance of the CART model is deemed valid. If these percentages had been above 80% (which assumes a 20% false alarm rate), then the model would be

considered excellent. However, the false alarm level is strictly user organization directed and dependent on the DoD assets at each operating location.

In addition to the results from the primary target classification trees, the alternate target classification trees (CH OUT, CAT STSS, and CAT STDS) showed interesting outcomes. Categorical speed and directional shear as well as channel outflows were also considered as target variables. Although the channel outflow predictor did not yield results which were better than the primary target, categorical shear confirmed the criteria JTWC uses for favorable and unfavorable conditions. It was shown that the criteria of 15 kts and 45 degrees of shear can be now applied to the 1000-200 mb level versus only the surface-200 mb level. This validation provides an increase in the understanding of the intricacies of tropical cyclone intensification.

## *5.2 Recommendations*

*5.2.1 Recommendations to JTWC.* CART analyses provide insightful information based on large databases and a variety of predictors. However, given the unique nature of the data mining process, the analyses provide a set of trees with varying degrees of size and accuracy (percent error misclassification and prediction success). In this research, the optimal tree, which minimized the percent error misclassification across all of the classes, was comprised of 25 terminal nodes. In addition, the splitting rules which led to the 25 terminal nodes varied among seven predictors, and the splitting rule path for each terminal node was unique. Although this technique was powerful in extracting every possible split in the data to produce a forecast decision path, it did not provide a concise

set of rules. Therefore, a generalization of the splitting rules was made, and a suggested set of splitting rules was established based on target class. This suggested set focused heavily on the CART analyses, however it still relies on sound meteorology when a CART split is considered unrealistic. The decision to utilize a CART splitting rule is based on the overall distribution of parameters in each target class. This technique assumed that conditions which promoted intensification trends in the past would dictate intensification trends in the future.

It is recommended that JTWC employ the results of the CART data mining software as a second-tier forecasting tool. The main emphasis should still reside in consensus model forecasting, and the critical predictors from the CART analyses should provide guidance towards which atmospheric parameters promote rapid intensification trends. In addition, the database required to maximize performance optimally needs thousands of records, of which to create a multitude of typhoon seasons would be required. However, it is believed that CART would also be an extremely useful tool in establishing a climatology of typhoon intensification events. If modeled data from the past decade could be included in the database, the overall predictability and accuracy of the CART model would increase.

If the overall objective had been to have a single set of rules from which to base typhoon intensification decisions, CART would not be the model of choice. However, as the objective is to learn more about the atmospheric state, then apply that knowledge to consensus model forecasting, CART is a superior tool. By examining each of the terminal nodes for class purity and splitting rules, very useful relationships can be

extracted. These relationships should enhance the decision making processes involved with numerical models.

*5.2.2 Future Research Recommendations.* The methodology and overall collection of the data introduced errors in the research. First, NOGAPS fields are output on a 2.5 x 2.5 degree grid, and this spacing yields approximately 150 nm between grid points. In order to ascertain the exact location of the typhoon, a finer resolution model would be needed. Currently, this grid point domain does not provide enough resolution to accurately capture the center of a typhoon (assuming core diameter ~ 20 to 30 nm). In addition, the teleconnection indices did not exactly match the regions covered by the typhoons. An interpolation scheme to better match the aerial coverage of the typhoons is needed and/or different teleconnection indices should be used. As of the present time, no teleconnection indices are known to cover the wide expanses of the Pacific Ocean over which typhoons traverse.

Second, the initial CART analyses integrated only 1198 records. This software is designed to data mine hundreds of thousands of records and works best when as many records as possible are input into the system. Less occurrences of Class 2 (7.26% of the total population) and Class 1 (6.18% of the total population) events resulted in prediction success scores of 78.16% and 86.49%, respectively, and misclassification rates of 21.84% and 13.51%, respectively. More Class 0 events (86.56% of the total population) resulted in a prediction success score of 70.88% and a misclassification rate of 29.12%. Thus, it is assumed that incorporating more data would increase the predictive power of CART.

Finally, better interpretation of subjective predictors would improve the overall performance of the research. Numerous typhoons had equatorial outflow channels, however a closed contour upper level anticyclone was not always observed (contrary to a circulation in the wind barb field). Therefore some skepticism about the actual influence existed. Adding another predictor, such as UC might pick up some of the influences noted by channel outflows, which are not specifically related to TUTT. The TUTT generally remained in the central Pacific, and it did not directly impact more western Pacific typhoons (indicative of LN regimes). A new predictor based on potential vorticity maximum (PVMAX) or major shortwave trough (MSWT) could account for interactions occurring without an accompanying channel outflow. The current methodology ignored these interactions since the focus was more towards TUTT influences versus PVMAX or MSWT.

The overall ability of CART to data mine every possible split in a large data set is impressive, and this ability should be exploited in conjunction with sound meteorology. The FSR only included the largest class populations in the terminal nodes, leaving behind the terminal nodes with only one or a couple of cases. Nevertheless, it was the synergy of just a few predictors which provided the most information leading to intensification and weakening trends. Since there were many ways to approach the analysis of the data, a key driver in this research was to maintain low percent error misclassification rates. Since lower error rates yielded larger trees, the FSR was developed to account for this condition. On the whole, the analyses did provide insightful information as to the predictors responsible for tropical cyclone intensification, and it is recommended that JTWC should include this information in their forecast process.

## Appendix A: MATLAB Linear Interpolation of Grid Points Program

This is the MATLAB code used to find the closest latitude and longitude grid point for each storm fix in the best track data.

```
clear
clc
format bank

% Read in the data and delete irrelevant columns
% Ensure no character data in .txt file
data = textread('filename.txt');
% 1997 data has 14 columns
% 1999 and 2001 data has 13 columns
data(:,11:13) = [];

% Assign values into different arrays
year = data(:,1);
month = data(:,2);
day = data(:,3);
hour = data(:,4);
lat = data(:,5);
lon = data(:,6);
spd = data(:,7);
dir = data(:,8);
winds = data(:,9);
pressure = data(:,10);

% Defining latitude and longitude gridpoints
gridlat = [0,2.5,5,7.5,10,12.5,15,17.5,20,22.5,25,27.5,30 ...
32.5,35,37.5,40,42.5,45,47.5,50];
gridlat = gridlat';
Egridlon = [180,177.5,175,172.5,170,167.5,165,162.5 ...
160,157.5,155,152.5,150,147.5,145,142.5 ...
140,137.5,135,132.5,130,127.5,125,122.5 ...
120,117.5,115,112.5,110,107.5,105,102.5 ...
100,97.5,95,92.5,90,87.5,85,82.5,80];
Wgridlon = [-120,-122.5,-125,-127.5,-130,-132.5 ...
-135,-137.5,-140,-142.5,-145,-147.5,-150,-152.5 ...
-155,-157.5,-160,-162.5,-165,-167.5,-170,-172.5 ...
-175,-177.5,-180,-182.5];
Egridlon = Egridlon';
Wgridlon = Wgridlon';
```

```

% Running interpolation on longitude
j = 1;
i = 1;
a = size(lon);
numlonrows = a(1);

for j = 1:numlonrows
    if lon(j) > 0
        while lon(j) <= ((Egridlon(i+1)+Egridlon(i)) / 2)
            i = i + 1;
        end
        glon(j) = Egridlon(i);
        j = j + 1;
        i = 1;
    else
        while lon(j) <= ((Wgridlon(i+1)+Wgridlon(i)) / 2)
            i = i + 1;
        end
        glon(j) = Wgridlon(i);
        j = j + 1;
        i = 1;
    end
end
glon = glon';

% Running interpolation on latitude
b = size(lat);
numlatrows = b(1);
k = 1;
m = 1;
for k = 1:numlatrows
    while lat(k) >= ((gridlat(m+1)+gridlat(m)) / 2)
        m = m + 1;
    end
    glat(k) = gridlat(m);
    k = k + 1;
    m = 1;
end
glat = glat';

% Showing actual and gridded
lat
lon
glat
glon

```

## Appendix B: MATLAB Calculation of Wind Shear Program

This is the MATLAB code used to calculate the surface-200 mb, 1000-200 mb, and 850-200 mb wind shear for each six hourly fix. The data is taken from the CART predictors spreadsheet which has u and v wind components for the surface, 1000 mb, 850 mb and 200 mb.

```
clear
clc
format bank

% Reading in data and setting up individual arrays
data = textread('filename.txt');
sfc_u = data(:,1);
sfc_v = data(:,2);
thsn_u = data(:,3);
thsn_v = data(:,4);
e50_u = data(:,5);
e50_v = data(:,6);
two_u = data(:,7);
two_v = data(:,8);
xx = size(data);
rows = xx(1,1);

% Converting U and V from m/s to kts
sfc_u = sfc_u * 1.943;
sfc_v = sfc_v * 1.943;
thsn_u = thsn_u * 1.943;
thsn_v = thsn_v * 1.943;
e50_u = e50_u * 1.943;
e50_v = e50_v * 1.943;
two_u = two_u * 1.943;
two_v = two_v * 1.943;

% Calculating sfc wind speed (kts)
i = 1;
for i = 1:rows
    sfc_ff(i) = sqrt((sfc_u(i))^2 + (sfc_v(i))^2);
    i = i + 1;
end
sfc_ff = sfc_ff;
```



```

% Calculating 1000 mb wind speed (kts)
i = 1;
for i = 1:rows
    thsn_ff(i) = sqrt((thsn_u(i))^2 + (thsn_v(i))^2);
    i = i + 1;
end
thsn_ff = thsn_ff';

% Calculating 850 mb wind speed (kts)
i = 1;
for i = 1:rows
    e50_ff(i) = sqrt((e50_u(i))^2 + (e50_v(i))^2);
    i = i + 1;
end
e50_ff = e50_ff';

% Calculating 200 mb wind speed (kts)
i = 1;
for i = 1:rows
    two_ff(i) = sqrt((two_u(i))^2 + (two_v(i))^2);
    i = i + 1;
end
two_ff = two_ff';

% Calculating sfc-200 mb speed shear (kts)
i = 1;
for i = 1:rows
    stss(i) = sqrt((two_u(i)-sfc_u(i))^2 + (two_v(i)-sfc_v(i))^2);
    i = i + 1;
end
stss = stss';

% Calculating 1000-200 mb speed shear (kts)
i = 1;
for i = 1:rows
    ttss(i) = sqrt((two_u(i)-thsn_u(i))^2 + (two_v(i)-thsn_v(i))^2);
    i = i + 1;
end
ttss = ttss';

% Calculating 850-200 mb speed shear (kts)
i = 1;
for i = 1:rows
    etss(i) = sqrt((two_u(i)-e50_u(i))^2 + (two_v(i)-e50_v(i))^2);
    i = i + 1;
end

```

```

end
etss = etss';

% Calculating sfc wind direction
i = 1;
for i = 1:rows
    if sfc_v(i) >= 0
        theta = 180;
    elseif sfc_u(i) < 0 && sfc_v(i) < 0
        theta = 0;
    elseif sfc_u(i) >= 0 && sfc_v(i) < 0
        theta = 360;
    end
    ddr_sfc(i) = atan(sfc_u(i) / sfc_v(i));
    sfc_dd(i) = ((ddr_sfc(i) / 3.1415927) * 180) + theta;
    if sfc_dd(i) > 360
        sfc_dd(i) = sfc_dd(i) - 360;
    end
    i = i + 1;
end
sfc_dd = sfc_dd';

% Calculating 1000 mb wind direction
i = 1;
for i = 1:rows
    if thsn_v(i) >= 0
        theta = 180;
    elseif thsn_u(i) < 0 && thsn_v(i) < 0
        theta = 0;
    elseif thsn_u(i) >= 0 && thsn_v(i) < 0
        theta = 360;
    end
    ddr_thsn(i) = atan(thsn_u(i) / thsn_v(i));
    thsn_dd(i) = ((ddr_thsn(i) / 3.1415927) * 180) + theta;
    if thsn_dd(i) > 360
        thsn_dd(i) = thsn_dd(i) - 360;
    end
    i = i + 1;
end
thsn_dd = thsn_dd';

% Calculating 850 mb wind direction
i = 1;
for i = 1:rows
    if e50_v(i) >= 0

```

```

        theta = 180;
    elseif e50_u(i) < 0 && e50_v(i) < 0
        theta = 0;
    elseif e50_u(i) >= 0 && e50_v(i) < 0
        theta = 360;
    end
    ddr_e50(i) = atan(e50_u(i) / e50_v(i));
    e50_dd(i) = ((ddr_e50(i) / 3.1415927) * 180) + theta;
    if e50_dd(i) > 360
        e50_dd(i) = e50_dd(i) - 360;
    end
    i = i + 1;
end
e50_dd = e50_dd';

% Calculating 200 mb wind direction
i = 1;
for i = 1:rows
    if two_v(i) >= 0
        theta = 180;
    elseif two_u(i) < 0 && two_v(i) < 0
        theta = 0;
    elseif two_u(i) >= 0 && two_v(i) < 0
        theta = 360;
    end
    ddr_two(i) = atan(two_u(i) / two_v(i));
    two_dd(i) = ((ddr_two(i) / 3.1415927) * 180) + theta;
    if two_dd(i) > 360
        two_dd(i) = two_dd(i) - 360;
    end
    i = i + 1;
end
two_dd = two_dd';

% Calculating sfc-200 mb directional shear
i = 1;
for i = 1:rows
    if two_dd(i) > sfc_dd(i)
        if two_dd(i) - sfc_dd(i) <= 180
            stds(i) = two_dd(i) - sfc_dd(i);
        end
        if two_dd(i) - sfc_dd(i) > 180
            stds(i) = (360 - two_dd(i)) + sfc_dd(i);
        end
    end
end
end

```

```

if sfc_dd(i) > two_dd(i)
    if sfc_dd(i) - two_dd(i) <= 180
        stds(i) = sfc_dd(i) - two_dd(i);
    end
    if sfc_dd(i) - two_dd(i) > 180
        stds(i) = (360 - sfc_dd(i)) + two_dd(i);
    end
end
end
i = i + 1;
end
stds = stds';

% Calculating 1000-200 mb directional shear
i = 1;
for i = 1:rows
    if two_dd(i) > thsn_dd(i)
        if two_dd(i) - thsn_dd(i) <= 180
            ttlds(i) = two_dd(i) - thsn_dd(i);
        end
        if two_dd(i) - thsn_dd(i) > 180
            ttlds(i) = (360 - two_dd(i)) + thsn_dd(i);
        end
    end
    if thsn_dd(i) > two_dd(i)
        if thsn_dd(i) - two_dd(i) <= 180
            ttlds(i) = thsn_dd(i) - two_dd(i);
        end
        if thsn_dd(i) - two_dd(i) > 180
            ttlds(i) = (360 - thsn_dd(i)) + two_dd(i);
        end
    end
end
i = i + 1;
end
ttlds = ttlds';

% Calculating 850-200 mb directional shear
i = 1;
for i = 1:rows
    if e50_dd(i) > sfc_dd(i)
        if e50_dd(i) - sfc_dd(i) <= 180
            etlds(i) = e50_dd(i) - sfc_dd(i);
        end
        if e50_dd(i) - sfc_dd(i) > 180
            etlds(i) = (360 - e50_dd(i)) + sfc_dd(i);
        end
    end
end

```

```

end
if sfc_dd(i) > e50_dd(i)
    if sfc_dd(i) - e50_dd(i) <= 180
        etds(i) = sfc_dd(i) - e50_dd(i);
    end
    if sfc_dd(i) - e50_dd(i) > 180
        etds(i) = (360 - sfc_dd(i)) + e50_dd(i);
    end
end
end
i = i + 1;
end
etds = etds';

% Displaying individual arrays of shear values
sfc_u
sfc_v
sfc_ff
sfc_dd
thsn_u
thsn_v
thsn_ff
thsn_dd
e50_u
e50_v
e50_ff
e50_dd
two_u
two_v
two_ff
two_dd
stss
ttss
etss
stds
ttds
etds

```

## Appendix C: Complete Set of Splitting Rules

This is the complete listing of splitting rules and number of records per terminal node. The splitting rules are the same regardless of class assignment, and this appendix should be used with Figure 23 to obtain an overall awareness of the classification tree.

<u>Terminal Node</u>	<u>Number of Records</u>	<u>Splitting Rule</u>
1	61	SFC T $\leq$ 26.89 & AGE $\leq$ 13.5
2	13	SFC T $\leq$ 26.89 & AGE > 13.5 & AGE $\leq$ 45.5 & LAT $\leq$ 13
3	13	SFC T $\leq$ 26.89 & AGE > 13.5 & AGE $\leq$ 45.5 & LAT > 13 & SST $\leq$ 18.5
4	108	SFC T $\leq$ 26.89 & AGE > 13.5 & AGE $\leq$ 45.5 & LAT > 13 & SST > 18.5
5	2	SFC T $\leq$ 26.89 & AGE > 45.5 & LAT $\leq$ 17.35
6	97	SFC T $\leq$ 26.89 & AGE > 45.5 & LAT > 17.35
7	206	SFC T > 26.89 & E50 T $\leq$ 18.99 & LAT $\leq$ 17.7
8	25	SFC T > 26.89 & E50 T $\leq$ 18.99 & LAT > 17.7 & AGE $\leq$ 17

9	27	SFC T > 26.89 & E50 T $\leq$ 18.99 & AGE > 17 & LAT > 17.7 & LAT $\leq$ 31.45
10	1	SFC T > 26.89 & E50 T $\leq$ 18.99 & AGE > 17 & LAT > 31.45
11	75	E50 T > 18.99 & AGE $\leq$ 36.5 & SFC T > 26.89 & SFC T $\leq$ 31.89 & LAT $\leq$ 13.15
12	16	E50 T > 18.99 & SFC T > 26.89 & SFC T $\leq$ 31.89 & LAT > 13.15 & LAT $\leq$ 21.35 & MEI $\leq$ 2.589 & AGE $\leq$ 5.5
13	104	E50 T > 18.99 & SFC T > 26.89 & SFC T $\leq$ 31.89 & LAT > 13.15 & LAT $\leq$ 21.35 & MEI $\leq$ 2.589 & AGE > 5.5 & AGE $\leq$ 36.5 & TWO T $\leq$ -47.81
14	16	E50 T > 18.99 & SFC T > 26.89 & SFC T $\leq$ 31.89 & LAT > 13.15 & LAT $\leq$ 21.35 & MEI $\leq$ 2.589 & AGE > 5.5 & AGE $\leq$ 36.5 & TWO T > -47.81

15	41	E50 T > 18.99 & AGE $\leq$ 36.5 & SFC T > 26.89 & SFC T $\leq$ 31.89 & LAT > 13.15 & LAT $\leq$ 21.35 & MEI > 2.589
16	87	E50 T > 18.99 & LAT $\leq$ 21.35 & AGE $\leq$ 36.5 & SFC T > 31.89
17	92	SFC T > 26.89 & E50 T > 18.99 & LAT $\leq$ 21.35 & AGE > 36.5 & SST $\leq$ 28 & MEI $\leq$ 2.6325
18	23	SFC T > 26.89 & E50 T > 18.99 & LAT $\leq$ 21.35 & AGE > 36.5 & SST $\leq$ 28 & MEI > 2.6325
19	15	SFC T > 26.89 & E50 T > 18.99 & LAT $\leq$ 21.35 & AGE > 36.5 & SST > 28
20	54	SFC T > 26.89 & E50 T > 18.99 & LAT > 21.35 & SST $\leq$ 23.5
21	18	SFC T > 26.89 & E50 T > 18.99 & LAT > 21.35 & SST > 23.5 & AGE $\leq$ 14.5



22	29	SFC T > 26.89 & E50 T > 18.99 & LAT > 21.35 & SST > 23.5 & AGE > 14.5 & MEI $\leq$ -0.239
23	24	SFC T > 26.89 & E50 T > 18.99 & LAT > 21.35 & AGE > 14.5 & MEI > -0.239 & SST > 23.5 & SST $\leq$ 26.45
24	21	SFC T > 26.89 & E50 T > 18.99 & LAT > 21.35 & AGE > 14.5 & MEI > -0.239 & SST > 26.45 & TWO T $\leq$ -49.31
25	30	SFC T > 26.89 & E50 T > 18.99 & LAT > 21.35 & AGE > 14.5 & MEI > -0.239 & SST > 26.45 & TWO T > -49.31

## Acronyms

AFCCC	Air Force Combat Climatology Center
AFWA	Air Force Weather Agency
AMS	American Meteorological Society
ATCF	Automated Tropical Cyclone Forecasting
BF	Banding Features
BOM	Bureau of Meteorology
BT	Best Track
CART	Classification and Regression Tree
CAT	Categorical
Cb	Cumulonimbus
CDO	Central Dense Overcast
CF	Central Features
CI	Current Intensity
CPC	Climate Prediction Center
Cu	Cumulus
D	Double Channel Outflow
EN	El Niño
FGGE	First GARP Global Experiment
FLENUMMETOC	Fleet Numerical Meteorology and Oceanography
FSR	Forecast Splitting Rules
GPH	Geopotential Height
GTCCA	Global Tropical Cyclone Climatic Atlas
IPV	Isentropic Potential Vorticity
JTWC	Joint Typhoon Warning Center
LN	La Niña
MEI	Multivariate ENSO Index
MPI	Maximum Potential Intensity
MSE	Mean Squared Error
MSLP	Minimum Sea Level Pressure
MSWT	Major Shortwave Trough
MWS	Maximum Wind Speed
N	No Channel Outflow
NCDC	National Climatic Data Center
NCEP	National Centers for Environmental Prediction
NH	Northern Hemisphere
NOGAPS	Navy Operational Global Atmospheric Prediction System
NRL	Naval Research Laboratory
NU	Neutral
PV	Potential Vorticity
PVMAX	Potential Vorticity Maximum
PVU	Potential Vorticity Unit

RC	Relative Cost
RH	Relative Humidity
RMSE	Root Mean Squared Error
S	Single Channel Outflow
S <sub>E</sub>	Single Channel Outflow (Equatorward)
S <sub>P</sub>	Single Channel Outflow (Poleward)
SAFA	Systematic Approach to Tropical Cyclone Forecasting Aid
SFCTMP	Surface Temperature
SH	Southern Hemisphere
SOI	Southern Oscillation Index
SST	Sea Surface Temperature
TC	Tropical Cyclone
TD	Tropical Depression
TS	Tropical Storm
TUTT	Tropical Upper Tropospheric Trough
UC	Upper Cyclone
UTC	Coordinated Universal Time
UTFT	Upper Tropospheric Flow Transitions
WISHE	Wind Induced Surface Heat Exchange

## Bibliography

- Benz, R.F. *Data Mining Atmospheric/Oceanic Parameters in the Design of a Long-Range Nephelometric Forecast Tool*. MS Thesis, AFIT/GM/03-02. School of Engineering Physics, Air Force Institute of Technology (AU), Wright-Patterson AFB OH, March 2003 (ADA412870).
- Black, P.G. and Shay, L.K., 1998: Air-sea interaction processes relevant to tropical cyclone intensity change. *Special Sessions on Tropical Cyclone Intensity Change*, AMS 78<sup>th</sup> Annual Meeting, Phoenix, AZ, 11-16 Jan, 1998.
- Bluestein, H.B., 1993: *Synoptic-Dynamic Meteorology in Midlatitudes, Volume II*. Oxford University Press, 594 pp.
- Bosart, L.F., Velden, C.S., Bracken, W.E., Molinari, J. and Black P.G., 2000: Environmental influences on the rapid intensification of Hurricane Opal (1995) over the Gulf of Mexico, *Monthly Weather Review*, **128**, 322-352.
- Breiman, L., Friedman, J.H., Olshen, R.A. and Stone, C.J., 1984: *Classification and Regression Trees*. Wadsworth, Belmont, CA, 358 pp.
- Chen, L. and Gray, W.M., 1985: Global view of the upper level outflow patterns associated with tropical cyclone intensity changes during FGGE, Dept. of Atmos. Sci., Paper No. 392, Colorado State University, Ft. Collins, CO, 118 pp.
- D'Aleo, J.S. and Grube, P.G., 2002: *The Oryx Resource Guide to El Niño and La Niña*. Oryx Press, 230 pp.
- Davidson, N.E. and Kar, S.K., 2002: Upper-tropospheric flow transitions during rapid tropical cyclone intensification, *Quarterly Journal of the Royal Meteorological Society*, **128**, 861-891.
- DeMaria, M., 1996: The effect of vertical shear on tropical cyclone intensity change, *Journal of the Atmospheric Sciences*, **53**, 2076-2087.
- Dvorak, V.F., 1974: Tropical cyclone intensity analysis and forecasting from satellite imagery, *Monthly Weather Review*, **103**, 420-430.
- Emanuel, K.A., 1986: An air-sea interaction theory for tropical cyclones. Part I: Steady-state maintenance, *Journal of the Atmospheric Sciences*, **43**, 585-604.
- Evans, J.L., 1993: Sensitivity of tropical cyclone intensity to sea surface temperature, *Journal of Climate*, **6**, 1133-1140.

- Ferreira, R.N. and Schubert, W.H., 1999: The role of tropical cyclones in the formation of tropical upper-tropospheric troughs, *Journal of the Atmospheric Sciences*, **56**, 2891-2584.
- Ford, B.W. *El Nino and La Nina Effects on Tropical Cyclones: The Mechanisms*. MS Thesis. Naval Postgraduate School (NPS), Monterey CA, June 2000 (ADA380280).
- Glickman, T.S., 2000: *Glossary of Meteorology*. American Meteorological Society, 855 pp.
- Global Tropical Cyclone Climatic Atlas, 2003: Tropical Cyclone Tracks 1997, 1999, and 2001 [Online at <http://navy.ncdc.noaa.gov/products/gtcca/gtccamain.html>].
- Goerss, J.S. and Jeffries, R.A., 1994: Assimilation of synthetic tropical cyclone observations into the navy operational global atmospheric prediction system, *Weather and Forecasting*, **9**, 557-576.
- Hanley, D., Molinari, J. and Keyser, D., 2001: A composite study of the interactions between tropical cyclones and upper-tropospheric troughs, *Monthly Weather Review*, **129**, 2570-2584.
- Holland, G.J., 1997: The maximum potential intensity of tropical cyclones, *Journal of the Atmospheric Sciences*, **54**, 2519-2541.
- Holliday, C.R. and Thompson, A.H., 1979: Climatological characteristics of rapidly intensifying typhoons, *Monthly Weather Review*, **107**, 1022-1034.
- Hoskins, B.J., McIntyre, M.E. and Robertson, A.W., 1985: On the use and significance of isentropic potential vorticity maps, *Quarterly Journal of the Royal Meteorological Society*, **111**, 877-946.
- Joint Typhoon Warning Center (JTWC) Website, 2003: TDO Handbook [Online at <https://pzal.npmoc.navy.mil/training/tдохandbook/TOC.htm>].
- Joint Typhoon Warning Center (JTWC) Website, 2003: TC Intensity Analysis Worksheet [Online at <https://pzal.npmoc.navy.mil/training/research/TCIntens.html>].
- Kelley, W.E., Jr. and Mock, D.R., 1982: A diagnostic study of upper tropospheric cold lows over the western North Pacific, *Monthly Weather Review*, **110**, 471-480.
- Kopp, T.J., 1995: *The Air Force Global Weather Central Surface Temperature Model*, Air Force Global Weather Central Technical Note 95/004, 23 pp.

- McNamara, T., 2001. The Dvorak Technique for tropical cyclone analysis. Advanced Synoptic Meteorology PowerPoint Presentation. Department of Engineering Physics, Air Force Institute of Technology, Wright-Patterson AFB, OH.
- Merrill, R.T., 1987: An experiment in the statistical prediction of tropical cyclone intensity change. NOAA Technical Memorandum, NWS, NHC 34, 33 pp.
- Merrill, R.T., 1988: Environmental influences on hurricane intensification, *Journal of the Atmospheric Sciences*, **45**, 1678-1687.
- Molinari, J., Skubis, S., Vollaro, D. and Alsheimer, F., 1998: Potential vorticity analysis of tropical cyclone intensification, *Journal of the Atmospheric Sciences*, **55**, 2632-2644.
- Montgomery, D.C. and Runger, G.C., 2002: *Applied Statistics and Probability for Engineers*, 3<sup>rd</sup> Edition. John Wiley and Sons, Inc., 720 pp.
- Naval Research Laboratory (NRL) Website, 1998: TC Forecaster's Reference Guide [Online at <http://www.nrlmry.navy.mil/~chu/tropcycl.htm>].
- Nyoumura, Y. and Yamashita, H., 1984: On the central pressure change of tropical cyclones as a function of sea surface temperature and land effect, *Geophysical Magazine*, **41**, 45-59.
- Price, J.D. and Vaughan, G., 1992: Statistical studies of cut-off-low systems, *Annales Geophysicae*, **10**, 96-102.
- Randall, R.M. *Exploration of Teleconnection Indices for Long-Range Seasonal Temperature Forecasts*. MS Thesis, AFIT/GM/02-08. School of Engineering Physics, Air Force Institute of Technology (AU), Wright-Patterson AFB OH, March 2002 (ADA404188).
- Sadler, J.C., 1964: Tropical cyclones of the Eastern North Pacific as revealed by TIROS observations, *Journal of Applied Meteorology*, **3**, 347-366.
- Sadler, J.C., 1975: The upper tropospheric circulation over the global tropics, Dept. of Meteorology, University of Hawaii, Rep. UHMET 75-05, 35 pp.
- Sadler, J.C., 1978: Mid-season typhoon development and intensity changes and the tropical upper tropospheric trough, *Monthly Weather Review*, **106**, 1137-1152.
- Salford Systems, 1995: *Data Mining with Decision Trees: An Introduction to CART<sup>®</sup>*. San Diego, CA, 133 pp.
- Salford Systems, 2002: *CART<sup>®</sup> for Windows User's Guide*. San Diego, CA, 295 pp.

- Sikora, C.R., 1976: *An investigation of equivalent potential temperature as a measure of tropical cyclone intensity*, FLEWEACEN Technical Note JTWC 76-3, 12 pp.
- Steinberg, D. and Colla, P., 1995: *CART: Tree-structured nonparametric data analysis*. San Diego, CA: Salford Systems, 355 pp.
- Thorpe, A. J., 1986: Synoptic-scale disturbances with circular symmetry, *Monthly Weather Review*, **114**, 1384-1389.
- University Center for Atmospheric Research (UCAR) Website, 2004: NOGAPS 4.0 [Online at <http://meted.ucar.edu/nwp/pcu2/nogaps>].
- Vilpors, S. Techniques Development Officer, Joint Typhoon Warning Center, Hickam AB, Hawaii. Personal Correspondences. February - December 2003.
- Whitfield, M.B. and Lyons, S.W., 1992: An upper-level low over Texas during summer, *Weather and Forecasting*, **7**, 89-106.
- Wilks, D.S., 1995: *Statistical Methods in the Atmospheric Sciences*. Academic Press, 467 pp.

## **Vita**

Capt Jonathan Leffler was born in Phoenix, Arizona. He graduated from Canon City High School and graduated from the University of Northern Colorado with a Bachelor of Science degree in Meteorology. In 1997, he entered active duty after attending Officer Training School at Maxwell AFB, Alabama.

His first assignment was Wing Weather Officer for the 28<sup>th</sup> Operational Support Squadron, Ellsworth AFB, South Dakota. In 1999, Capt Leffler was assigned as Assistant Flight Commander, A-Flight, to the USAFE Operational Weather Squadron, Sembach AB, Germany. In 2001, he became Flight Commander of A-Flight. While serving in Germany, Capt Leffler qualified for Foreign Area Officer and attended the French Language and Area Studies Immersion Program in Nice, France. He was also selected to attend the Air Force Institute of Technology in 2002. Capt Leffler is married and has one daughter.



REPORT DOCUMENTATION PAGE				Form Approved OMB No. 074-0188	
<p>The public reporting burden for this collection of information is estimated to average 1 hour per response, including the time for reviewing instructions, searching existing data sources, gathering and maintaining the data needed, and completing and reviewing the collection of information. Send comments regarding this burden estimate or any other aspect of the collection of information, including suggestions for reducing this burden to Department of Defense, Washington Headquarters Services, Directorate for Information Operations and Reports (0704-0188), 1215 Jefferson Davis Highway, Suite 1204, Arlington, VA 22202-4302. Respondents should be aware that notwithstanding any other provision of law, no person shall be subject to a penalty for failing to comply with a collection of information if it does not display a currently valid OMB control number.</p> <p><b>PLEASE DO NOT RETURN YOUR FORM TO THE ABOVE ADDRESS.</b></p>					
1. REPORT DATE (DD-MM-YYYY) March 2004		2. REPORT TYPE Master's Thesis		3. DATES COVERED (From – To) Jun 2003 – Mar 2004	
4. TITLE AND SUBTITLE  FEASIBILITY OF USING CLASSIFICATION ANALYSES TO DETERMINE TROPICAL CYCLONE RAPID INTENSIFICATION				5a. CONTRACT NUMBER	
				5b. GRANT NUMBER	
				5c. PROGRAM ELEMENT NUMBER	
6. AUTHOR(S)  Leffler, Jonathan W., Captain, USAF				5d. PROJECT NUMBER	
				5e. TASK NUMBER	
				5f. WORK UNIT NUMBER	
7. PERFORMING ORGANIZATION NAMES(S) AND ADDRESS(S)  Air Force Institute of Technology Graduate School of Engineering and Management (AFIT/ENP) 2950 Hobson Way, Bldg 640 WPAFB OH 45433-7765				8. PERFORMING ORGANIZATION REPORT NUMBER  AFIT/GM/ENP/04-07	
9. SPONSORING/MONITORING AGENCY NAME(S) AND ADDRESS(ES)  Naval Pacific Meteorology and Oceanography Center/Joint Typhoon Warning Center 425 Luapele Road Pearl Harbor, HI 96860-3103				10. SPONSOR/MONITOR'S ACRONYM(S)	
				11. SPONSOR/MONITOR'S REPORT NUMBER(S)	
12. DISTRIBUTION/AVAILABILITY STATEMENT  APPROVED FOR PUBLIC RELEASE; DISTRIBUTION UNLIMITED.					
13. SUPPLEMENTARY NOTES					
14. ABSTRACT  Tropical cyclone intensity techniques developed by Dvorak have thus far been regarded by tropical meteorologists as the best identification and forecast schemes available using satellite imagery. However, in recent years, several ideologies have arisen which discuss alternative means of determining typhoon rapid intensification or weakening in the Pacific. These theories include examining channel outflow patterns, potential vorticity superposition and anomalies, tropical upper tropospheric trough interactions, environmental influences, and upper tropospheric flow transitions. It is now possible to data mine these atmospheric parameters thought partly responsible for typhoon rapid intensification and weakening to validate their usefulness in the forecast process. Using the latest data mining software tools, this study used components of NOGAPS analyses along with selected atmospheric and climatological predictors in classification analyses to create conditional forecast decision trees. The results of the classification model show an approximate $R^2$ of 0.68 with percent error misclassifications of 13.5% for rapidly weakening typhoon events and 21.8% for rapidly intensifying typhoon events. In addition, a merged set of suggested forecast splitting rules was developed. By using the three most accurate predictors from both intensifying and weakening storms, the results validate the notion that multiple parameters are responsible for rapid changes in typhoon development.					
15. SUBJECT TERMS  Classification and Regression Tree, CART, Tropical Cyclone Intensification, Typhoon Intensification					
16. SECURITY CLASSIFICATION OF:			17. LIMITATION OF ABSTRACT  UU	18. NUMBER OF PAGES  121	19a. NAME OF RESPONSIBLE PERSON Lt Col Ronald P. Lowther, ENP
a. REPORT U	b. ABSTRACT U	c. THIS PAGE U			19b. TELEPHONE NUMBER (Include area code) (937) 255-3636, ext 4645